CHALMERS
UNIVERSITY OF TECHNOLOGY

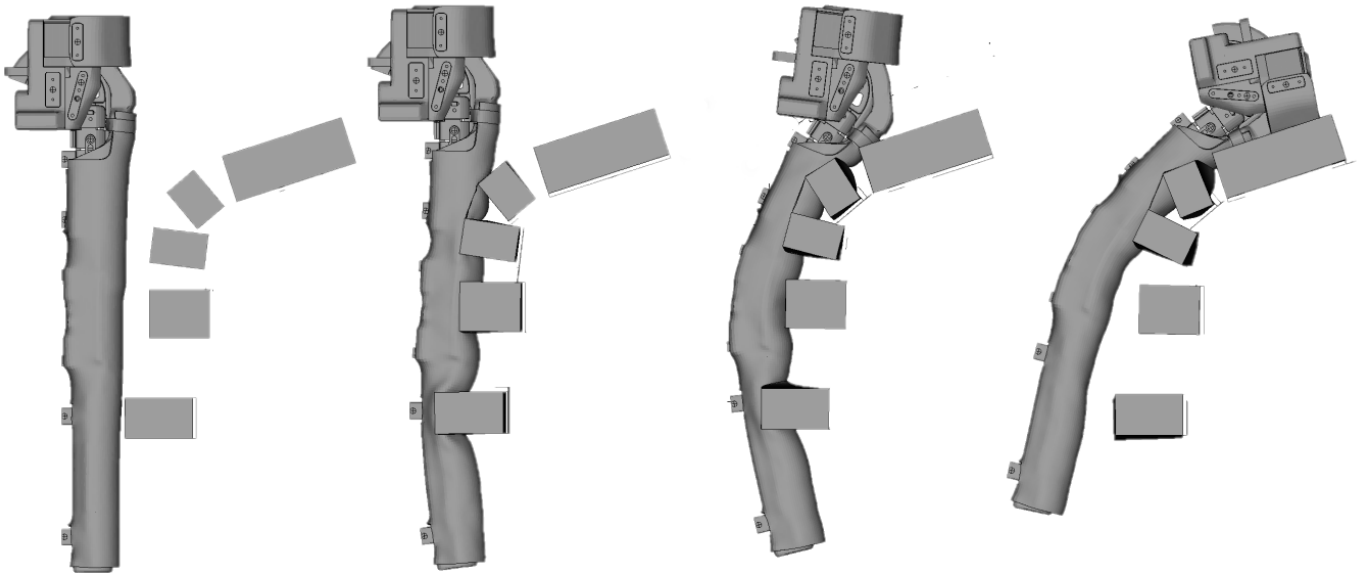

Evaluation of finite element models of the advanced Pedestrian Legform Impactor

Master's thesis in Mobility Engineering

AXEL GUTTMAN
DAVID RANDBY

DEPARTMENT OF MECHANICs AND MARITIME SCIENCES

CHALMERS UNIVERSITY OF TECHNOLOGY
Gothenburg, Sweden 2024
www.chalmers.se

Master's thesis in mobility engineering 2024

Evaluation of finite element models of the advanced Pedestrian Legform Impactor

AXEL GUTTMAN
DAVID RANDBY

CHALMERS
UNIVERSITY OF TECHNOLOGY

Department of Mechanics and Maritime Sciences
Division of Vehicle Safety
Chalmers University of Technology
Gothenburg, Sweden 2024

Evaluation of finite element models of the advanced Pedestrian Legform Impactor
AXEL GUTTMAN
DAVID RANDBY

Supervisor: Nils Olofsson, Volvo Cars
Examiner: Johan Davidsson, Mechanics and Maritime Sciences

Master's Thesis 2024
Department of Mechanics and Maritime Sciences
Division of Vehicle Safety
Chalmers University of Technology
SE-412 96 Gothenburg
Telephone +46 31 772 1000

Cover: A 3D model of the aPLI impacting the GVTR in the FE enviroment

Typeset in LaTeX
Printed by Chalmers Reproservice
Gothenburg, Sweden 2024

Evaluation of finite element models of the advanced Pedestrian Legform Impactor
AXEL GUTTMAN
DAVID RANDBY
Department of Mechanics and Maritime Sciences
Chalmers University of Technology

Abstract

According to the National Highway Traffic Safety Administration (NHTSA), 54,769 pedestrians were injured in the United States during 2020 (Stewart, 2023). Among these injured pedestrians, 12,623 experienced incapacitating injuries (National Center for Statistics and Analysis, 2022). To minimize such injuries, both physical and Finite Element (FE) representations of the advanced Pedestrian Legform Impactor (aPLI) are used in vehicle design to reduce the risk of serious injuries to the lower extremities. The physical aPLI is a mechanical representation of the human leg used to assess knee, tibia, and femur injury risk in crash testing. This project aimed to evaluate the performance of two different FE models of aPLIs in LS-DYNA by conducting dynamic validation tests. In addition, this project aimed to determine which FE aPLI model better correlated with physical test results using a Generic Vehicle Test Rig (GVTR) within the limitations set by this thesis.

A dynamic validation test was conducted on a physical aPLI to ensure its validity. The test employed an energy absorber attached to a linearly guided sled, which impacted the aPLI at 40 km/h. The resulting signal responses from sensors in the knee, tibia, and femur had to fall within a specified certification corridor for the physical aPLI to be considered valid. This test was then mimicked in the FE environment, and the performance of the FE aPLI models was evaluated based on how close to the physical test results they predicted. The two FE aPLI models were Humanetics v1.2.6 and ATD-models D02.11. A sensitivity study was conducted during this step of the project, in which the FE dynamic validation test was performed using the maximum and minimum tolerance limits to investigate if the signal responses from the FE aPLI models would diverge. The next step consisted of simulating impact tests with the GVTR and comparing the results to physical test results.

The results showed that the Humanetics FE aPLI model demonstrated better and more consistent performance in the validation test. It was slightly more robust in the FE sensitivity study and produced results that correlated more closely with physical impact tests with the GVTR.

Keywords: aPLI, FE, GVTR, Pedestrian, Leg impactor.

Preface

This thesis project is the base for a Master's degree in Mobility Engineering at Chalmers University of Technology. The work has been carried out at Volvo Cars Safety Centre in Torslanda, Gothenburg, Sweden during the spring of 2024.

Acknowledgements

We would like to begin by extending our heartfelt gratitude to everyone who supported us during our thesis project and our time at Chalmers University of Technology.

A special thank you to **Volvo Cars** and our supervisor **Nils Olofsson** for the opportunity to undertake our Master's thesis with you and for laying the foundation for it. Your unwavering support and invaluable insights have been instrumental throughout the entire project.

We also extend our sincere thanks to **Niklas Gråberg** and the **Pedestrian Safety Team** for their warm welcome and all the assistance provided. It has been a truly fun and educational experience.

Our appreciation also extends to **Anders Fredriksson** for his valuable input and expertise in the area.

We also thank **Jonas Östh** for his help with data analysis and for allowing us to visit volvo safety center and observe a full crash test.

Finally, we are deeply grateful to our examiner **Johan Davidsson** for accepting our project and allowing us to conduct this thesis.

Axel Guttman, David Randby, Gothenburg, May 2024

List of Acronyms

Below is the list of acronyms that have been used throughout this thesis listed in alphabetical order:

ACL	Anterior Cruciate Ligament
aPLI	Advanced Pedestrian Legform Impactor
ATD	Anthropomorphic Test Device
ATD-models	Softwarecompany providing FE-models of the aPLI
BM	Bending Moment
CAE	Computer Aided Engineering
CFC	Channel Frequency Class
EuroNCAP	European New Car Assessment Program
FE	Finite Element
FEM	Finite Element Method
FlexPLI	Flexible Pedestrian Legform Impactor
GVTR	Generic Vehicle Test Rig
HBM	Human Body Model
IC	Injury Criterion
IPF	Injury Probability Function
ISO	International Organization for Standardization
MCL	Medial Collateral Ligament
PCL	Posterior Cruciate Ligament
RES	Renewable-based Energy Sources
RMS	Root Mean Square
SMS	Selective Mass Scaling
VRU	Vulnerable Road Users
WIFac	Weighted Integrated Factor
WHO	World Health Organization

Contents

List of Figures

List of Tables

1
Introduction

According to the World Health Organization (WHO, 2023), approximately 1.19 million people die each year due to injuries sustained in traffic-related crashes based on worldwide data. More than half of these fatalities are among vulnerable road users (VRUs), including pedestrians, cyclists, and motorcyclists. The imbalance in mass and protection between pedestrians and vehicles creates an increased risk for pedestrians in collisions. Consequently, pedestrians account for 23% of all road-related fatalities (WHO, 2023). The body parts most prone to injury are the head, lower body, and legs. Leg injuries sustained in a pedestrian accident rarely lead to death but can result in hospitalization and permanent disability.

According to the National Highway Traffic Safety Administration (NHTSA, 2022), 54,769 pedestrians were injured in traffic-related crashes. Of the injured pedestrians, 12,623 experienced incapacitating injuries, which prevented them from walking, driving, or normally continuing everyday activities.

Passive pedestrian safety focuses on protecting pedestrians when an impact is unavoidable. This involves conducting FE simulations and physical tests using ATDs that represent the head, hip, or lower extremities. The primary goal of pedestrian safety testing is to enhance vehicle design to reduce the risk of severe injuries, fatalities, and minor injuries to pedestrians. Previous legform impactors could not adequately simulate the bending moment exerted on the femur due to the lack of upper body mass representation. Therefore, the development of a new legform impactor was initiated (Isshiki, T et al. 2016) to increase its biofidelity. The advanced Pedestrian Legform Impactor (aPLI) is now used in Euro NCAP testing to assess the risk of injury to the femur, knee, and tibia.

In the early stages of car design, Computer-Aided Engineering (CAE) is utilized long before a prototype can be built and crash-tested. Manufacturers use finite element solvers like LS-DYNA (Ansys®, R12.2.1, 2024) to simulate crash tests. For these simulations to be valuable during the design phase, it is crucial that the FE representations of ATDs yield results similar to those of their physical counterparts. Additionally, the FE models of vehicles must be accurately constructed to ensure realistic outcomes from the ATDs. An overly optimistic model may cause vehicles to underperform in physical tests, while an excessively conservative model can lead to higher costs and extended project timelines. Understanding the strengths and limitations of FE ATDs is essential for achieving robust and accurate crashworthiness assessments.

This thesis evaluated the performance of two FE aPLI models, one developed by Humanetics and the other by ATD-models. The FE aPLI models were assessed based on their performance in a simulated dynamic validation test. The physical dynamic validation test is used to validate the physical aPLI, ensuring that the bending moment output signals from the femur and tibia, as well as knee ligament elongation, remain within certification corridors (ISO 20458:2024). This test is performed by impacting a physical aPLI with an energy absorber (in this case, a honeycomb structure) attached to a linearly guided sled moving at 40 km/h. This test was replicated and simulated with the FE aPLI models, and their performance was evaluated based on how well the FE aPLI models output data matched the physical test data. Afterward, simulations were conducted on a Generic Vehicle Test Rig (GVTR), where the FE aPLI models impacted the GVTR at 40 km/h. The performance evaluation was also based on comparing the simulated results to the physical test results.

1.1 Aim

The aim of this project was to evaluate the performance of two different FE models of aPLI in LS-DYNA by conducting dynamic validation simulation tests and impact simulations against a Generic Vehicle Test Rig (GVTR). The performance of the FE aPLIs was assessed by comparing the simulated test results with the physical test results. The results of interest included the bending moments in the femur and tibia, as well as the elongation of the ligaments in the knee.

To achieve this aim, the following questions were investigated:

1. How well do the signal outputs in simulated dynamic tests compare to physical dynamic tests?
2. How well do the signal outputs from simulated impacts with a GVTR compare to physical impact tests with a GVTR?

1.2 Limitations

The FE aPLI models were already validated by their developers, and no modifications were made to the models during this project. In this thesis, the dynamic validation test was only simulated in the FE environment. The physical test data used for evaluating the performance of the FE aPLIs was obtained from the most recent physical validation of the aPLI. The energy absorber, an important structure of the validation test, was modeled according to the specifications set in ISO 20458:2024. Only eight physical tests were conducted on the GVTR for data gathering purposes.

2

Background

In this chapter, readers will explore an overview of FE modeling, including time step and mass scaling, and mesh convergence. The chapter will also cover the application of these concepts in pedestrian safety assessments, specifically focusing on dynamic validation procedures.

2.1 Finite Element Modeling

The FE method is a technique for numerically solving differential equations that typically arise in structural, thermal, and fluid modeling. In the vehicle industry, nonlinear FE analysis is essential for crash test simulations. FE simulations are replacing crash testing in evaluating designs in the early stages, material choices, details of the final design, and more. It provides a more rapid way of design evaluation at a lower cost compared to traditional engineering practices (Belytschko et al., 2014).

Different problem-solving algorithms are employed depending on the mathematical model that must be solved. For crash simulations with large deformations, an explicit solver is used. It solves the numerical problem by calculating the system's state in small time steps without iterating to equilibrium. Explicit FEM is crucial for crash testing. LS-DYNA, being the most widespread and one of the most used software for crash simulations and calculations, is also the preferred solver for this thesis.

For pre-processing and post-processing, ANSA (© BETA CAE Systems, R24.1.0, 2024) and META (© BETA CAE Systems, R23.1.3, 2024) was utilized, respectively. ANSA serves as pre-processing software, handling tasks such as geometry import and cleanup, automated mesh generation, material assignment and model assembly. META, on the other hand, functions as post-processing software, enabling the storage of simulation results in graphs and reports for effective interpretation. META also supports the creation of animations, allowing visualization of results in a 3D environment.

2.1.1 Time step and mass scaling

In explicit FE-simulations, a time step refers to a small increment of time utilized for calculations. This parameter plays a crucial role in dynamic simulations as it dictates the level of detail in the time domain. Choosing an appropriate time step is important to strike a balance between computational efficiency and accuracy. Increasing the critical time step can be achieved by utilizing equation (2.1), which determines the speed of sound through a material. By increasing the density of a material, c is increased, leading to a decrease of the wave propagation speed in the material, meaning a larger time step. This introduction of nonphysical mass is called mass scaling. The goal is to have a balance between computational efficiency and maintaining accurate simulation results (LS-Dyna Support, 2024).

$$c = \sqrt{\frac{E}{\rho}} \tag{2.1}$$

$$\triangle t = \frac{L}{c} \tag{2.2}$$

$\triangle t$ =Time step

L =Characteristic element length

c =Speed of sound in the material

ρ = Density of material

E = Young's modulus of material

2.1.2 Mesh convergence

Mesh convergence is the iterative process of refining the element size in the FE model until the output results are not effected by further refinement. As the mesh becomes finer, with more elements and nodes, the computational cost inevitably increases. The primary objective is to identify when mesh convergence is achieved. This is typically determined by visually observing and measuring deformations. When further refinement of the mesh fails to enhance simulation outcomes, it signifies that mesh convergence has been reached, rendering additional refinement unnecessary. However, it is important to note that acheiving mesh convergance does not guarantee the accuracy or the results, as other sources of error, such as incorrect boundary conditions, material models and friction may still be present in the model. In contrast to implicit FEM, the goal with explicit FEM is not to locally refine the mesh to capture stress concentrations, as doing so would lead to significant mass scaling

of these small local elements (Belytschko et al., 2014).

2.1.3 Hourglass energy

Hourglass energy refers to the energy linked with unintended hourglass deformations in finite element analysis. This energy is not physically meaningful and serves as a source of numerical error in simulations. Excessive hourglass energy can result in inaccuracies and instability in the analysis. These deformations typically arise due to inadequate mesh constraints or inaccuracies in representing material behavior.

2.2 Crash Tests

Vehicle crash tests are vital assessments aimed at determining a vehicle's crashworthiness. These tests involve controlled collisions conducted in a controlled environment, with specific load cases. Accelerometers are employed to gather data during these crashes. Additionally, sensors are installed on anthropomorphic test devices, commonly known as crash test dummies. These dummies are utilized to ensure repeatability, reproducibility, and to mimic the kinematic response of a human during crashes.

There are several different New Car Assessment Program (NCAP) that are active in Europe, Japan, USA, and several other nations. This thesis focuses on the Euro NCAP. They scrutinize vehicles with more rigorous crash tests compared to the crash tests designed for legal certification of the vehicles. NCAP rates vehicles on a scale of 1 to 5 stars, with 5 stars representing the highest level of safety. A vehicle that only meets the legal certification standards typically does not receive any stars in Euro NCAP testing. But with a 5-star rating from Euro NCAP, it signifies to consumers that the vehicle manufacturer has considered the safety of both pedestrians and occupants of the vehicle. Meaning that cars with a 5-star rating tend to attract consumer that value safety. This is one of the reasons why manufacturers conduct simulated crash tests early in the design phase, to validate or discard design choices based on their performance. Both full-scale crash tests with vehicle-to-barrier and subsystem tests such as pedestrian-leg impacting vehicle-front are conducted.

To assess crashes, injury risk can be calculated from the accelerations, force, displacement and other data gathered by sensors during the crash, evaluating the potential injuries sustained by a human occupant in the scenario. This injury risk must fall below a threshold value to pass certification. The injury criterion used to calculate the injury risk is derived from tests conducted on post-mortem human subjects and real-world crash reconstructions. While crash test dummies are continuously enhanced to achieve greater biofidelity and realism, this advancement also introduces increased complexity.

2.2.1 Pedestrian safety

Vulnerable Road Users (VRU) are defined by Euro NCAP (2024) as “non-motorized road users, including pedestrians, cyclists, motorcyclists, and individuals with disabilities or reduced mobility and orientation”. In tests conducted by Euro NCAP, the primary focus is on pedestrians and cyclists, where assessments include head impact, pelvis impact, and leg impact. These tests often involve reconstructions of scenarios typical in urban areas, as accidents between cars and VRU frequently occur at pedestrian crossings and at city speeds.

2.3 Legform Impactors

Pedestrian crash worthiness first started testing in 1987, initial computer simulations showed a better response from leg impactors compared to full size dummies when impact occurred below the knee. The first leg impactor consisted of 2 rigid cylinders covered in foam and synthetic skin connected with a joint to represent the knee. The knee joint would rotate and translate laterally. The impactor was instrumented with an accelerometer and a transducer that could measure the relative angular displacement of the cylinders representing the femur and the tibia to measure the elongation of the ligaments (Janssen, 1996). This impactor was proposed by the European Enhanced Vehicle-safety Committee in 1998. To improve the kinematics and biofidelity of the impactor, in 2002 organizations from Japan started researching an impactor that imitates the flexible nature of the human bones by replacing the rigid long bones with flexible bones constructed in segments where bending moment can be measured in these segments across the bones (Isshiki, T et al., 2016), resulting in the Flexible Pedestrian Legform Impactor (Flex-PLI). In this design, the knee joint is enhanced, with the knee comprising two aluminum blocks representing the tibia and femur. These blocks are connected by four springs, symbolizing the ligaments in a typical knee joint. (Han et al. 2018).

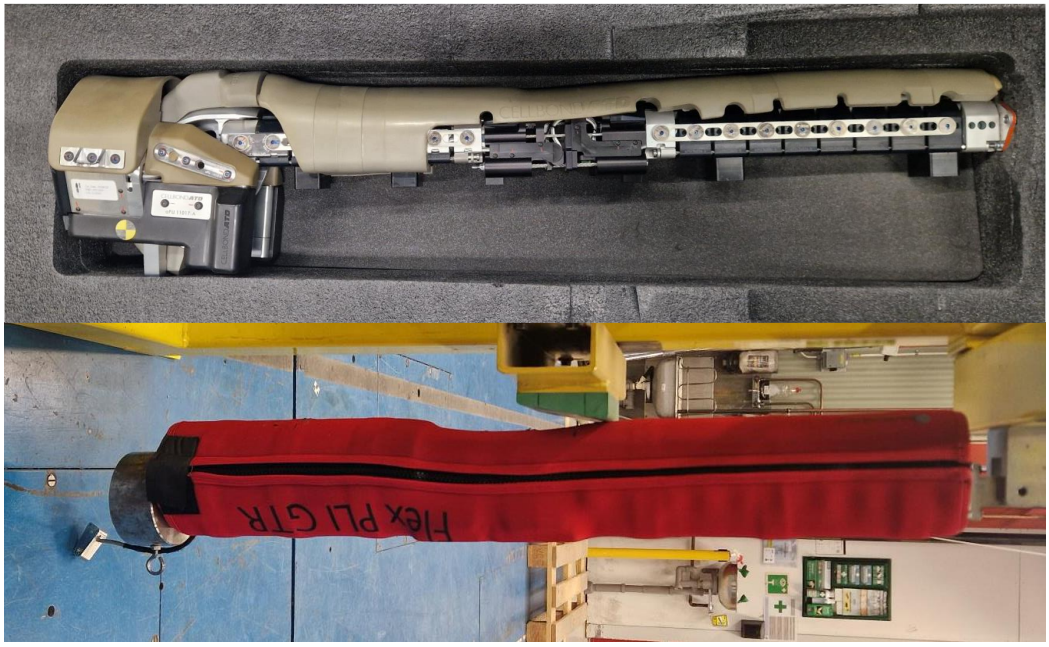

Figure 2.1: Photo of the aPLI (above) without skin and the Flex-PLI (below) with flesh and skin.

Despite its improved capabilities over the previous legform impactor, the Flex-PLI was still unable to adequately assess femur injury risk. As a result, a separate upper legform impactor was employed for this purpose. To enhance the biofidelity of the Flex-PLI, the development of a new legform impactor was initiated (Isshiki, T et al., 2016). Research demonstrated that refining the specifications of the Flex-PLI FE model and adding a biofidelic simplified upper body part significantly improved the impactor's biofidelity. This new impactor was the first development of the advanced Pedestrian Leg Impactor (aPLI) (Isshiki, T et al., 2016). Due to the aPLI's enhanced representation of the human leg, EuroNCAP (Euro NCAP, 2023) is considering discontinuing the separate assessment of upper and lower legforms, as was done with the Flex-PLI (Autoliv, 2023), and adopting the aPLI as the sole test case for pedestrian leg impact.

2.4 Advanced Pedestrian Legform Impactor

The aPLI, serves as a mechanical representation of a human leg for simulating vehicle to pedestrian crashes and assessing the risk of pedestrian injuries. The enhanced kinematics and biofidelity of the aPLI depend significantly on its composition, consisting of various components that together form distinct sub-assemblies, ultimately creating the fully assembled aPLI. The different sub-assemblies represents the various parts of the human leg that are of interest for evaluating risk of injury.

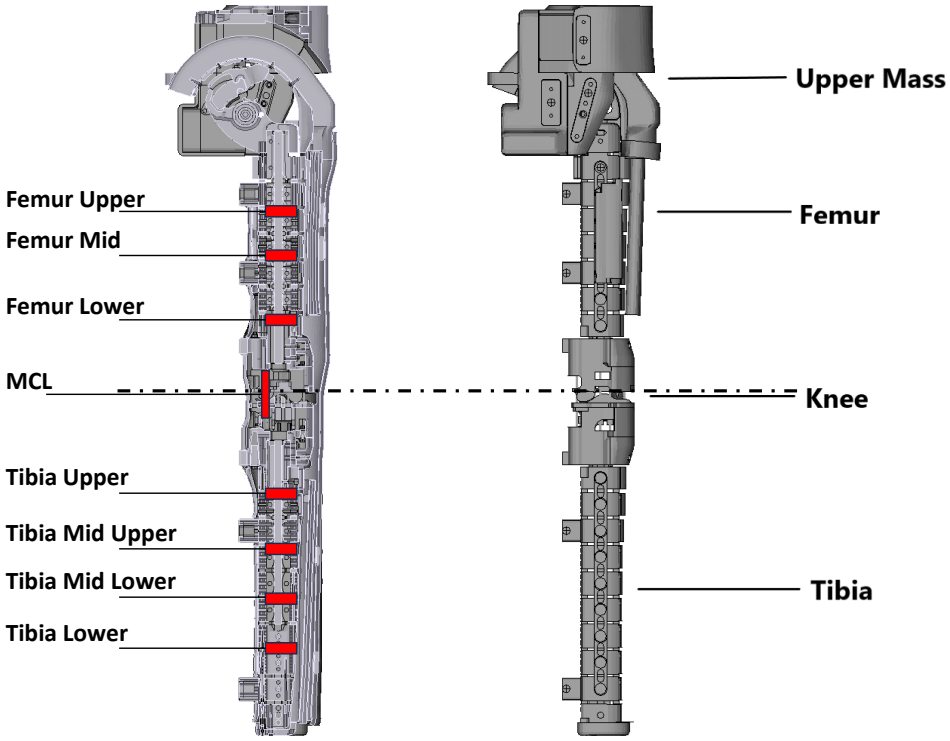

Figure 2.2: Crosscut of the Humanetics FE aPLI model showing the location of the sensors to the left. To the right is the Humanetics FE aPLI model without the skin and flesh.

2.4.1 Upper Mass

This part is the most prominent difference between the aPLI and the earlier Flex-PLI. The upper mass represents the inertia of the upper body during a vehicle to pedestrian crash, making the kinematics of the simulation more realistic and improving the injury assessment capability. The increased biofidelity from the upper mass further enhances accuracy of the results and enables evaluation of injuries in the thigh region. The upper mass assembly shall have a mass of $11.8 \pm 0.3kg$.

2.4.2 Femur

Inside the femur of the aPLI, a core that is made from glass-fiber reinforced plastic represents the bone structure. It is important for the core to show a bending stiffness closely resembling that of a human long bone. The key values of interest in the femur include the bending moment (BM), which is derived by measurements of the strain near the core and then converting it to obtain the bending moment.

2.4.3 Knee

The knee joint consists of 2 stiff aluminum blocks that represent the femoral condyles and tibia plateau. They are connected by steel wires and springs that imitate the MCL, ACL and PCL. The elongation of all ligaments is measured but MCL

elongation is only considered when risk of injury is calculated due to it being at highest risk of injury, Asgari. M., Keyvanian. Sh.S, (2019)

2.4.4 Tibia

The core material inside the tibia is the same glass-fiber reinforced plastic as for the femur. Similar to the femur, the core of the tibia needs a bending stiffness closely to that of a human. The bending moment for the tibia is the key value of interest and is derived in the same way as for the femur.

2.4.5 Flesh And Skin

The flesh encapsulates all the other sub systems, the flesh consists of one layer of material and the skin is the outer most layer and consists of a sheet of polychloroprene and a fabric surface.

2.5 Dynamic validation test

The aPLI calibration and validation process is conducted in several steps. The first step involves performing component level tests at a subsystems level and calibrating them individually. This calibration primarily focuses on the internal sensors. Once the sensors are calibrated to ensure correct response and accuracy, the leg can be validated in a full-assembly validation rig. This rig is a one-dimensional impact sled that impacts the aPLI with a linearly guided sled. At the front of the impact carriage an energy absorber is placed, consisting of a honeycomb block in aluminum 5052 that can handle a crush strength of up to 517 kPa and have a tolerance of $\pm 34.5\ kPa$. In the premises where the calibration test will take place, the indoor temperature needs to be 20 $\pm$ 2 degrees Celsius and the relative humidity inside needs to be $40\% \pm 30\%$. The output data from the full-assembly impact test needs to stay within the certification corridor (ISO/TS 20458:2023, edition 1) more detail on the values can be seen in section 2.5.3. Because of how the calibration and validation of the aPLI is structured, calibrating the sub assemblies first and then validating the entire assembly, once the full assembly is validated (produces outputs that stay within the certification corridor) the leg is valid. This means that the aPLI can be calibrated nominal (close to the center of the corridor) more sensitive (high in the corridor) less sensitive (low in the corridor).

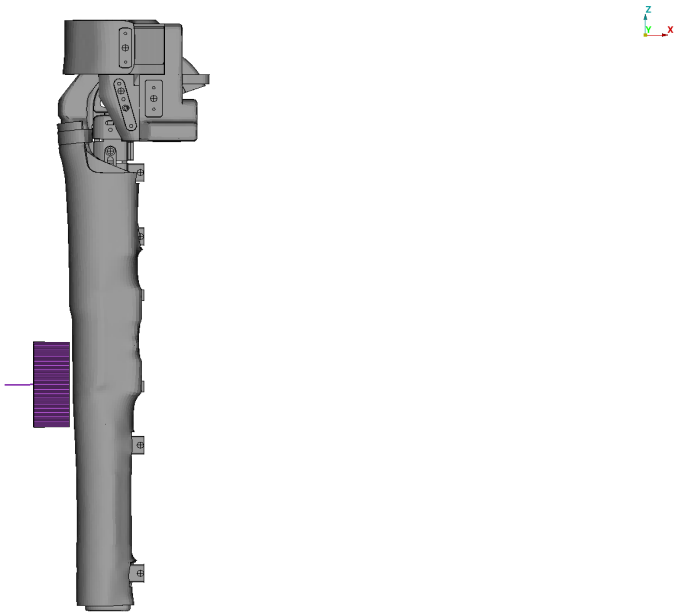

Figure 2.3: Schematic over the FE model of the dynamic validation test with Humanetics FE aPLI model (to the left) and honeycomb energy absorber (to the right).

2.5.1 Impact cases

There are two different impact cases associated with the dynamic validation test. The difference between the impact cases is the height of which the honeycomb impacts the aPLI. For Type 1, the sled and honeycomb impacts the aPLI below the knee and for Type 2, the sled and honeycomb impacts the aPLI directly at the knee.

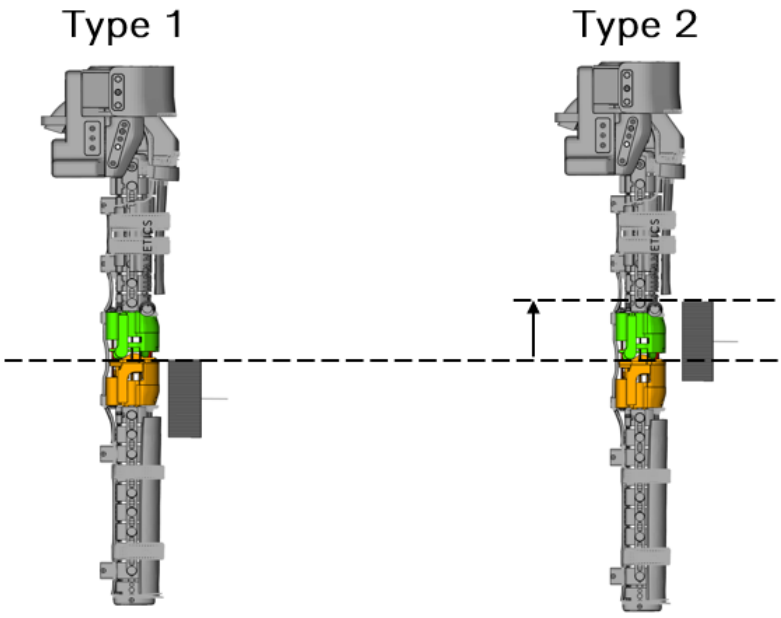

Figure 2.4: Impact cases Type 1 left and Type 2 right, Highlighted in green and orange is the upper and lower parts of the knee (Humanetics aPLI in both figures).

2.5.2 Test equipment requirements, validation test

Table 2.1 outlines requirements specified in the ISO standard that need to be fulfilled for the physical validation test. These requirements should be followed during validation tests conducted within both the FE environment and physical environment to ensure replicability. Using these specified values simplifies the process of reproducing the test. For material stiffness the crush strength has been recalculated to the force needed to attain the correct crush strength.

Table 2.1: Certification criteria for test equipment

Parameter	Assessment Conditions	Requirement
Impact carriage mass	Including honeycomb block	8,15 kg ± 0,1 kg
Impact velocity	Measured less than 20 mm before impact	11,1 m/s ± 0,2 m/s
Impact height Type 1	Impact below knee (see fig 2.2)	0 ± 2 mm
Impact height Type 2	Impact on knee (see fig 2.2)	120 mm ± 2 mm
Material stiffness	Honeycomb crush strength	16.4 kN ± 10%

2.5.3 Certification corridor, validation test

The aPLI must fulfill two distinct certification corridors for approval, corresponding to the impact cases Type 1 and Type 2. When simulating an impact, ten output

signals are measured, and for approval, the maximum measured value from each signal must fall within the respective corridor, as can be seen in table 2.2 and 2.3.

The certification corridors were established using a TF method, which involved initially creating IPFs for humans. These IPFs were then transformed into ones for the aPLI in specific load cases through regression analysis comparing maximum injury metric values between humans and aPLI. Then adjustments were made after evaluating their relevance against real-world accident data. Any notable disparities led to modifications aimed at improving alignment with real-world scenarios.

Table 2.2: Certification specifications of full-assembly certification tests (Type 1 impact below knee)

Corridor	BM [Nm]							Elongation [mm]		
	Femur-UP	Femur-MID	Femur-LO	Tibia-UP	Tibia-MID-UP	Tibia-MID-LO	Tibia-LO	ACL	PCL	MCL
Upper	136,0	182,0	213,0	339,0	278,0	194,0	115,0	4,00	7,60	16,50
Lower	103,0	135,0	165,0	299,0	245,0	163,0	92,0	3,20	5,70	12,10

Table 2.3: Certification specifications of full-assembly certification tests (Type 2 impact at knee)

Corridor	BM [Nm]							Elongation [mm]		
	Femur-UP	Femur-MID	Femur-LO	Tibia-UP	Tibia-MID-UP	Tibia-MID-LO	Tibia-LO	ACL	PCL	MCL
Upper	193,0	243,0	300,0	249,0	231,0	163,0	83,0	4,00	9,70	24,40
Lower	145,0	190,0	234,0	211,0	187,0	134,0	65,0	2,80	7,80	20,30

2.6 Legform to Bumper Test

The Euro Ncap legform to bumper test focusess on pedestrian safety utilizing a legform impactor to simulate a pedestrian being struck by a vehicle traveling at 40 km/h. A schematic view of the impact can be seen in figure 2.6. The hight of the aPLI from the ground when impact between the vehicle and aPLI occurs is $25mm$. This test was conducted physicaly with the GVTR for data gathering pourposess and simulated with the FE aPLI models to evaluate the performance of the models.

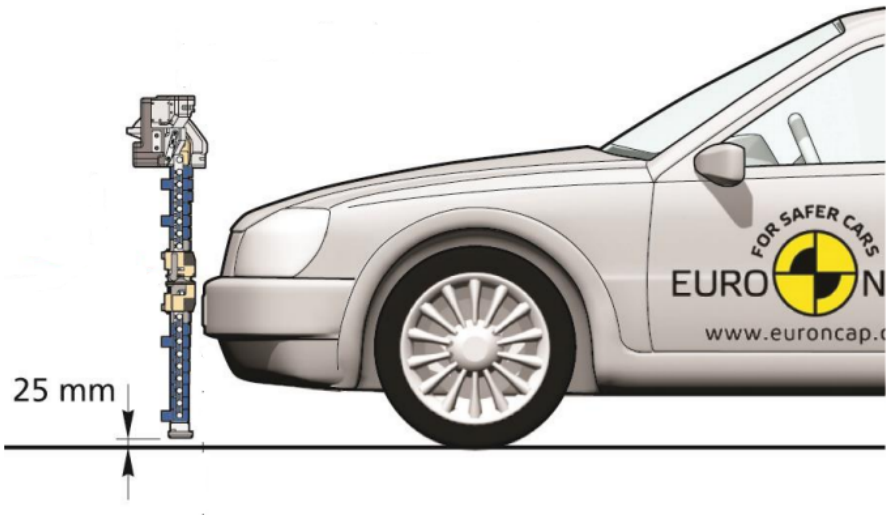

Figure 2.5: Schematic view of the legform to bumper test (Euro NCAP, 2024)

2.6.1 Generic Vehicle Test Rig

The GVTR that was used for this thesis was designed to mimic a generic midsize SUV. Increasing the height of the rig mimmics the height of the vehicle. The physical GVTR is comprised of foam blocks

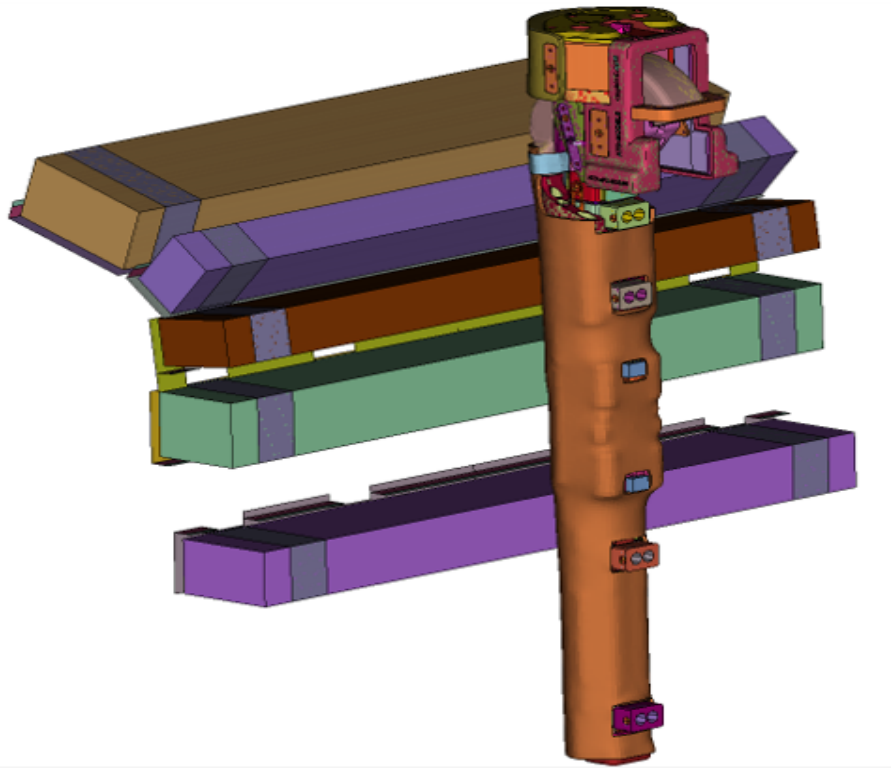

Figure 2.6: Figure of the ATD FE aPLI model and GVTR FE model.

2.7 Humanetics FE aPLI model

One of the FE aPLI models that will be investigated for this thesis is Humanetics aPLI version 1.2.6. Humanetics specializes in designing, manufacturing, and supplying ATDs for the automotive industry and regulatory safety organizations to evaluate and enhance vehicle safety standards. Humanetics also provide simulation software models and calibration equipment (Humanetics, 2024). With their FE aPLI model, they include the Borderline tool which allows users to adjust eight input signals for the two impact cases, Type 1 and Type 2. This tool can be used to change the calibration of the FE aPLI model to simulate different calibrations of the physical aPLI. For instance, if an engineer wants to simulate an FE aPLI that mimics a physical aPLI calibrated to be more sensitive (high in the certification corridor), they could input the maximum allowed value in the tool to achieve this. The tool primarily changes stiffness properties in the material models used in the FE model. Adjusting one signal often affects the other signals. The tool assists users by displaying both certification corridors and boundary values, which dynamically adjust based on other input values.

The responses generated by the aPLI, following adjustments made with the Borderline tool, should exhibit a deviation of less than four percent (Humanetics, 2024). This means that the desired output should closely match the input.

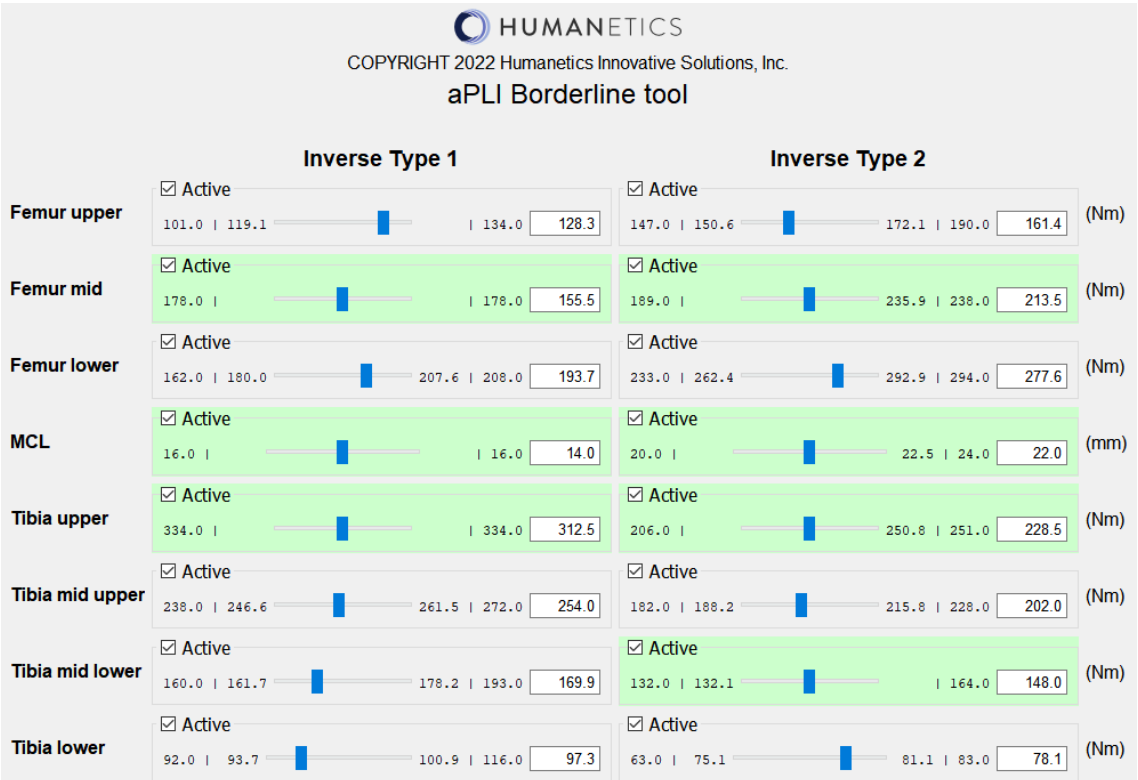

Figure 2.7: The *Borderline tool* included with the aPLI version 1.2.6 from Humanetics.

The signals with green background are the primary/independent target and should be set first. The signals with grey background are the secondary/dependent targets and should be set secondly. The tool generates a parameter-file that will be used in the simulations.

2.8 ATD-models

The other FE aPLI model that will be evaluated is ATD-models aPLI version d02.11. ATD-models specializes in FE computational models for vehicle crash and occupant simulations (ATD-models, 2024). ATD-models does not offer the possibility for the user to tune the aPLI. The leg comes as a plug-and-play with regular uppdates that further improve the correlation of the impactor.

2.9 Evaluation of the FE apli models

The evaluation of the two FE aPLI models was conducted by first simulating the dynamic validation test on both FE aPLIs and compare their results to the results from the lates physical dynamic validation test. The FE aPLI models were also simulated in a legform to bumper test where a GVTR was used to represent a vehicle. The FE results were compared to physical test results performed during the thesis.

2.10 Physical calibration of aPLI

The latest validation test was conducted by a company specialized in measurement technology and took place in November 2023. The results from these dynamic validation tests are presented in tables A.1 and A.2, which include the measured values for each part along with their specification corridor. The aPLI tested successfully and met all certification corridors outlined by Euro NCAP, which were established in April 2021. However, it's noteworthy that updated versions of the certification corridors for Type 1 and Type 2 were released in 2024, as illustrated in A.3.

3
Methods

The chapter outlines the methods used to achieve the aim of this thesis. To evaluate the FE aPLI models, two different simulation setups were employed. The first simulation setup was a digital version of the dynamic validation test (see 2.5), where the performance of the FE aPLI models was compared to test results from a physical test on an aPLI, as well as how sensetive the FE aPLI models were to changes in the boundary conditions of the dynamic validation test. The second simulation setup involved a legform to bumper test (see 2.6), in which a FE GVTR model was struck by the FE aPLI models. The FE aPLI models were assessed by comparing their results from simulations with the results from physical legform to bumper tests.

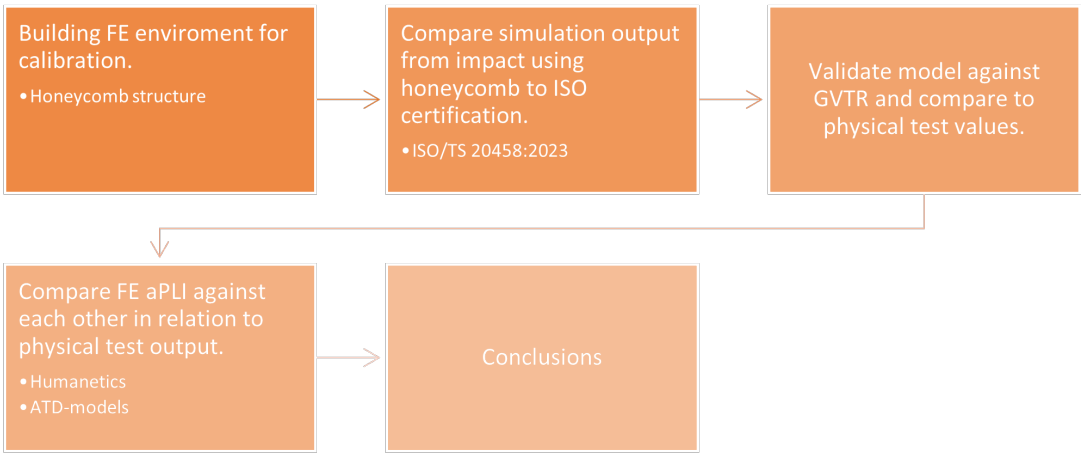

Figure 3.1: Workflow of the project.

3.1 Building the dynamic validation FE model

To evaluate which FE aPLI model would perform best compared to the physical aPLI, a virtual dynamic validation test model was developed. The boundary conditions and setup of the virtual model were based on the physical validation test

(see 2.5). The component-level tests conducted on the physical leg were not simulated because the FE aPLI models could not be disassembled into sub-assemblies to conduct these tests.

3.1.1 Honeycomb structure

The virtual honeycomb structure was designed to meet the nominal performance stated in ISO/TS 20458:2023, and thus no physical tests will be conducted on a honeycomb energy absorber during this thesis. Instead, a virtual crush test was performed where a force was applied to the honeycomb structure to ensure thet the structure would crush at the correct preassure.

The first objective in building the calibration FE model was to validate the performance of the honeycomb energy absorber, which consists of a block of 5052 aluminum sheets arranged to form an internal pattern of hexagonal cylindrical spaces. While the physical honeycomb block had small inconsistencies in the cell composition, as seen in Figure 3.2a, modeling these inconsistencies was deemed too time-consuming for this thesis. Instead, a symmetrical honeycomb structure was modeled in ANSA, as shown in Figure 3.2b with the same cell size of $4,75mm$.

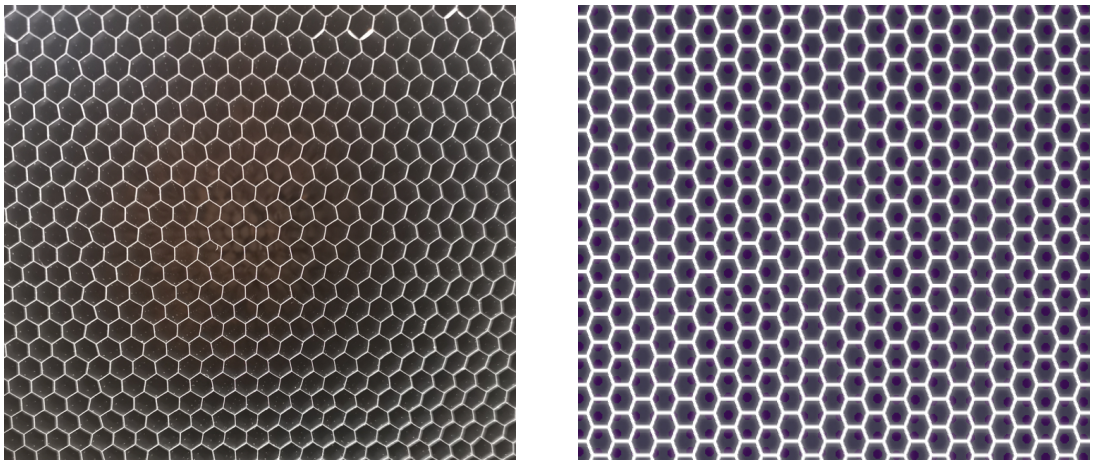

(a) Irregurarly slanted honeycomb. **(b)** FE modeled symetrical honeycomb.

Figure 3.2: Figures displaying the difference of the real vs FE honeycomb.

The next step in building the honeycomb structure was to achieve mesh convergence. This was done by refining the element shape and size to obtain deformations and buckling that correspond to the real honeycomb energy absorber. Initial simulations started with quadrilateral element with a size of 2.7 mm, as seen in Figure 3.3a, and triangular elements that split the quad elements diagonally creating double the amount of elements, as shown in Figure 3.3b. The structure created using triangular elements exhibited a better buckling shape compared to the one created using quadrilateral elements, which bulged outward. The difference in buckling shape can be seen in Figure 3.3c and 3.3d. This improvement may be attributed to the increased number of elements as well as the change in element shape. No clear choice of element shape could be decided on with these simulations.

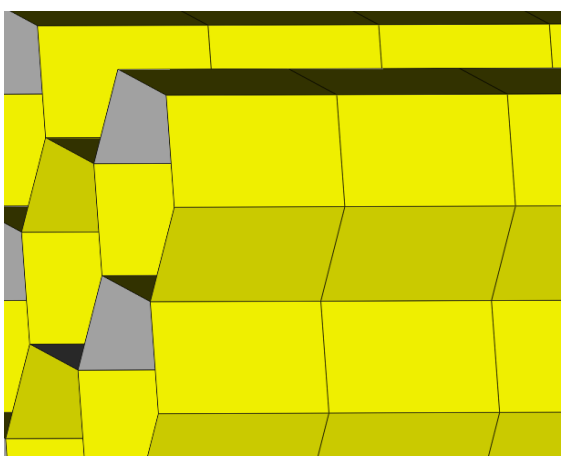

(a) First quadratic element.

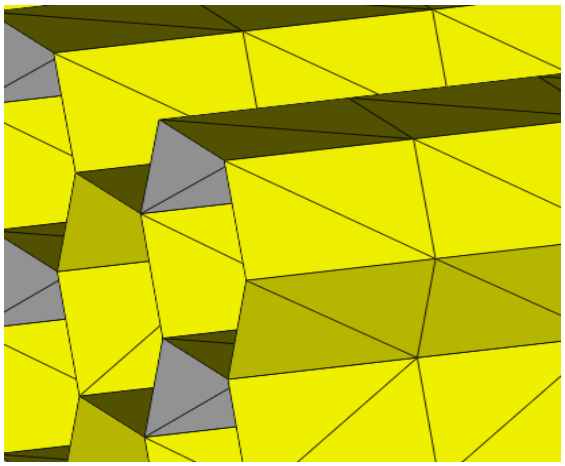

(b) First triangular element.

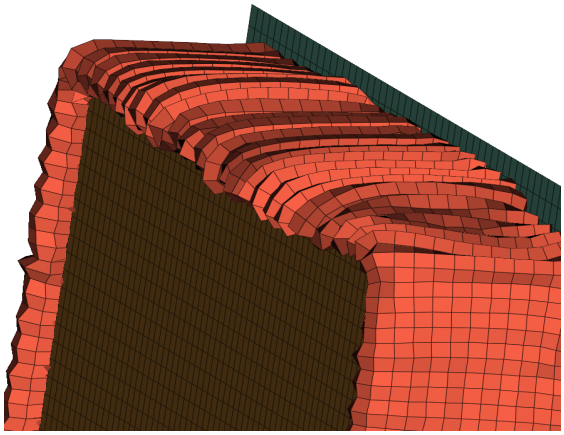

(c) First quadratic element deformation.

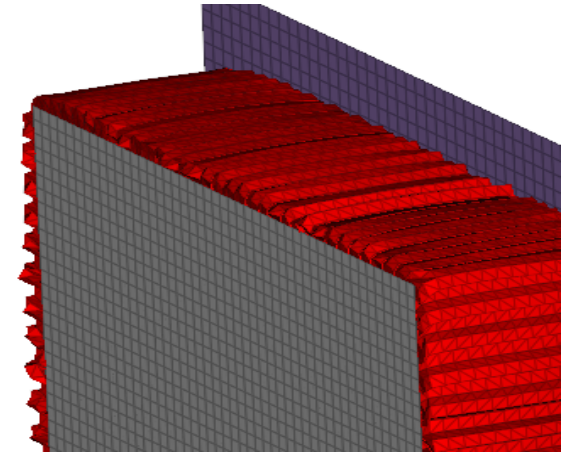

(d) First triangular element deformation.

Figure 3.3: Initial simultion element shape size and deformations.

Further simulations were conducted with a refined mesh for both element shapes. The refined element size can be seen in figure 3.4a and 3.4b. Both models showed improved buckling deformations, characterized by a lack of outward bulging, and the structure deforming by first crimpling the outer wall and later imploding as the structure crushed. The model with quadrilateral elements had half the number of elements and a faster computation time. However, this model exhibited high proportions of hourglass energy. The model with triangular elements displayed favorable buckling characteristics and did not exhibit problems with hourglass energy. Therefore, triangular elements with an edge length of $1.2mm$ were selected for further simulations. Although triangular elements with smaller sizes were experimented with, they mostly increased computational time without showing improvements in deformations. As a result, they were not pursued further.

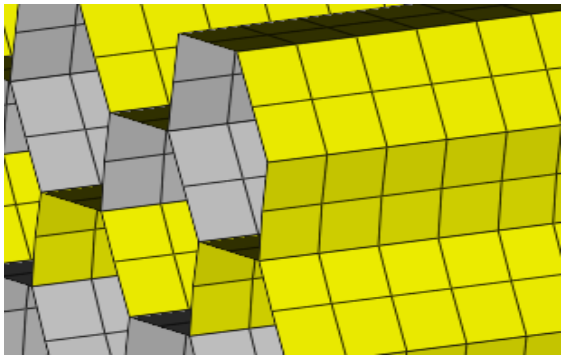

(a) Refined quadratic element.

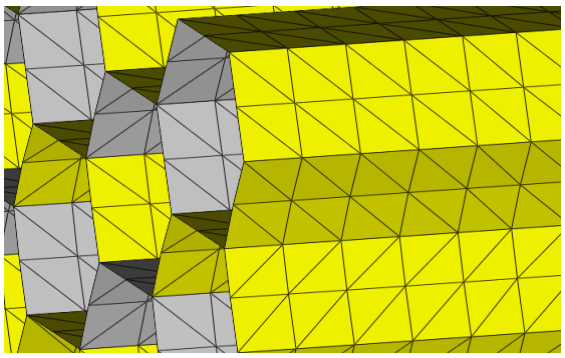

(b) Refined triangular element.

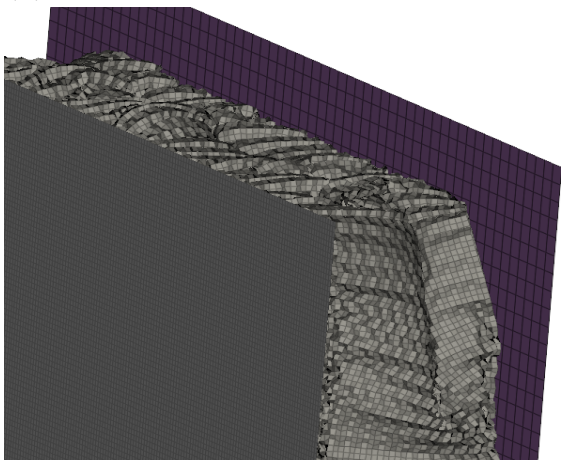

(c) Refined quadratic element deformation.

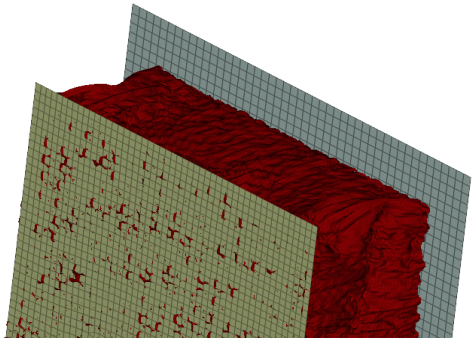

(d) Refined triangular element deformation.

Figure 3.4: Refined simulations element shape size and deformations.

After selecting the shape and size of the element, an iteration over the wall thickness began to determine the correct crush strength of the energy absorber. This process utilized a crush setup, wherein the honeycomb was connected to a sled that applied a force, pressing the honeycomb into a rigid wall seen in Figure 3.5a. The force exerted increased exponentially in effort to keep the simulation time from becoming to long, as illustrated in Figure 3.5b, the green region on the graph outlines the force

within which the honeycomb should crush to remain within the crush tolerance set by the ISO standard.

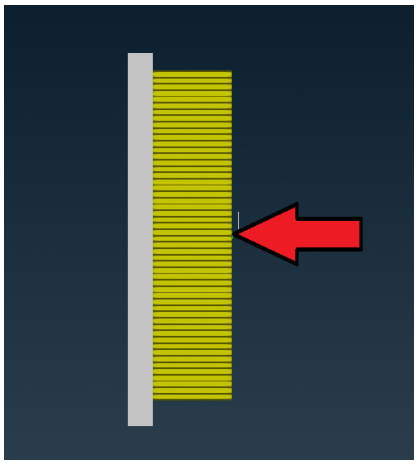

(a) Schematic over honeycomb validation setup.

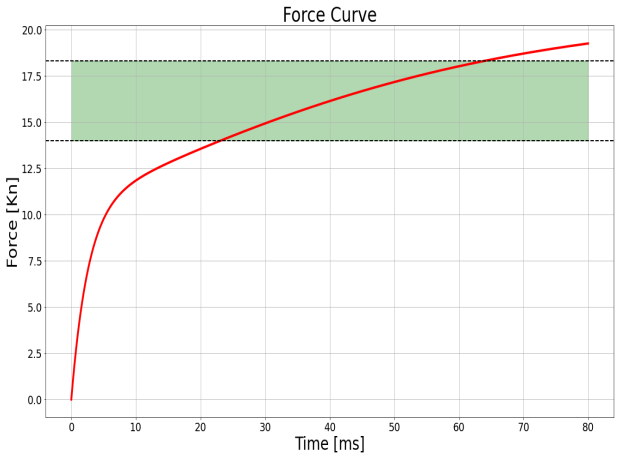

(b) Normalized force curve.

Figure 3.5: Figures displaying a scematic over the validation setup and load curve.

The wall thickness needed to fulfill the crush strength set by the ISO standard was $0,007mm$. The force that crushes the honeycomb is measured at a cross section in the honeycomb, a comparison of the load curve and the crush curve can be seen in figure 4.1. The decision to use the crush strength approach for the honeycomb structure was driven by the need to keep the model simple and require less computational power. Increasing the wall thickness would necessitate the use of smaller elements to maintain realistic kinematics. However, smaller elements would significantly increase computational power requirements and simulation time.

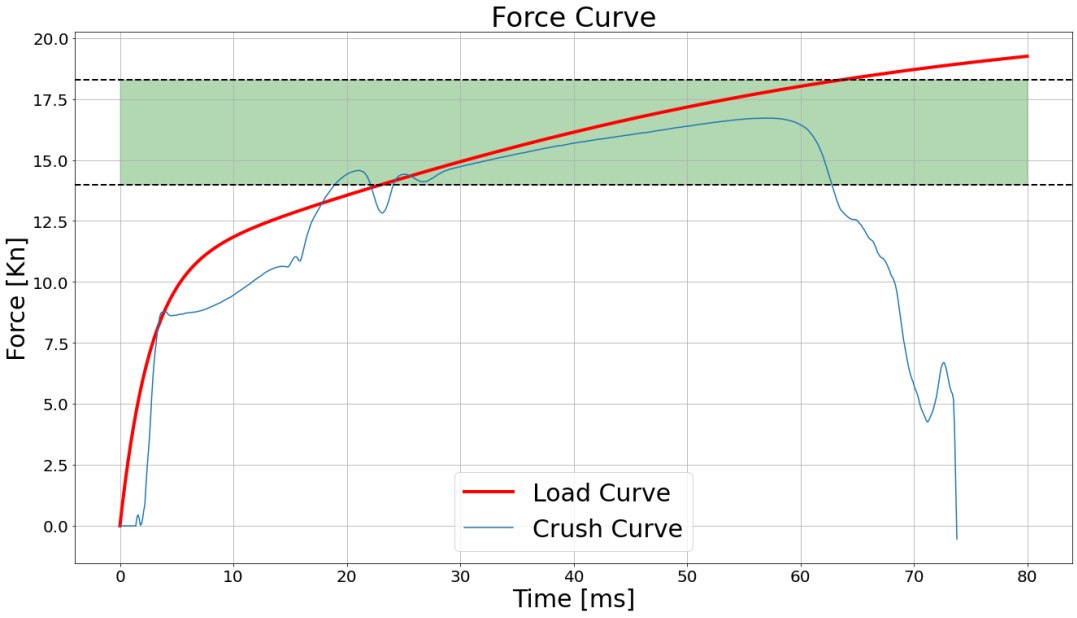

Figure 3.6: Load curve in red and crush curve for the honeycomb in blue.

3.1.2 Boundary conditions sled

In the FE calibration model, the sled serves as a simplified representation of the physical calibration rig. It features a rigid back wall with two overhanging edges above and below the honeycomb and a mounted beam on the backside. The edges prevent the honeycomb from falling due to gravity, while the beam allowed manipulation of the impact carriage's Center of Gravity (C.O.G). Like its physical counterpart, the FE sled was constrained to move in a single direction, aligning with the constraints observed in the actual calibration rig.

3.2 Dynamic validation simulations

After the honeycomb structure was validated for simulation, the simulations progressed to the dynamic validation test. The setup and boundary conditions for this test are elaborated in Section 2.5. The relevant boundary condition, where the honeycomb moved only in the x-direction, was configured in ANSA to replicate the test environment. The dynamic validation test was selected as a primary benchmark for the FE aPLI models due to the availability of physical test data for comparison with simulated results. The test environment adhered to ISO/TS 20458:2023, providing clear instructions for all boundary conditions. The honeycomb structure was the sole variable that could potentially affect the outcome. An illustration of how the dynamic validation simulation looked before impact is shown below 3.7.

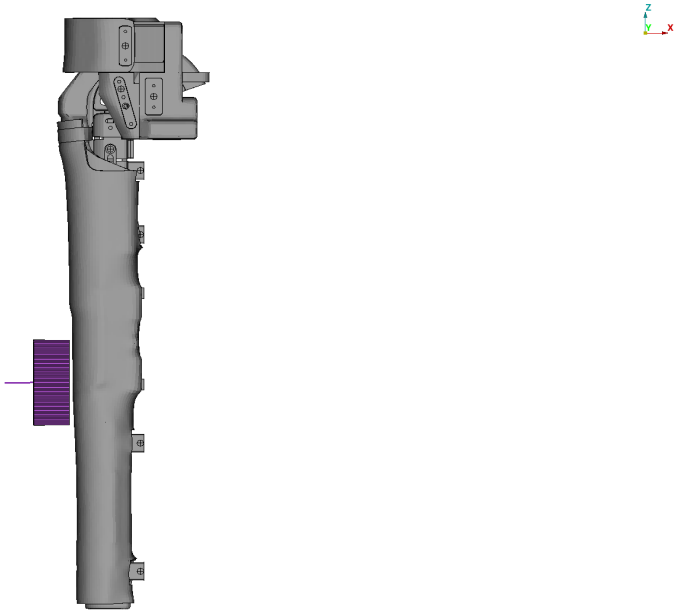

Figure 3.7: An illustration of how the dynamic validation simulation looked like before impact.

3.2.1 Calibration settings for Humanetics FE aPLI model in the Borderline software

When deciding on the calibration approach for the Humanetics FE aPLI model, two directions were considered. The first approach involved calibrating the FE aPLI model to a midpoint within the available corridor. In this scenario, the borderline tool would be adjusted so all parameters would align with the middle of the corridor, with further adjustments based on the signal response from the simulated validation test. In figure 3.8b, shows an example of the femur middle signal overshooting the middle of the corridor and where adjustments needed to be made in the borderline tool to align better with the desired value. This method was selected as the baseline calibration for the FE aPLI model. Alternatively, the second approach was calibrating the Humanetics FE aPLI model to match the physical aPLI used in this thesis. Lab reports from the latest calibration of the aPLI were used as the desired value, seen in figure 3.8b

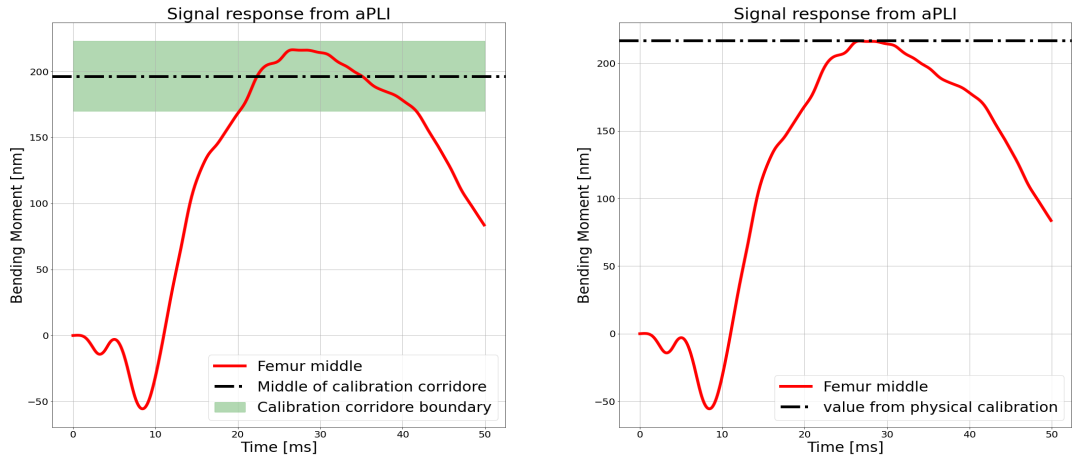

(a) Borderline calibration alternative 1. **(b)** Borderline calibration alternative 2.

Figure 3.8: Figures displaying signal response for calibration purpose.

3.2.2 Evaluation of borderline tool using output from physical validation test

To assess the reliability of the honeycomb structure and the precision of the borderline tool, simulations were conducted using the output values obtained from physical calibration tests as inputs for the borderline tool. By comparing them against each other, one could obtain figures on the deviation the humanetics FE aPLI model has from the physical tests and an indication of which direction the Humanetics FE aPLI model should be adjusted to better match the physical validation outputs using the borderline tool.

3.2.3 Optimizing FE-simulations

Optimizing the simulation time for the honeycomb structure was necessary due to initial simulations taking up to 20 hours to complete. To reduce simulation

time without compromising accuracy, simulations with Selective Mass Scaling (SMS) were conducted and compared to simulations without mass scaling. All elements within the honeycomb were mass scaled. A small difference in the results was documented, but it was decided to continue simulations with mass scaling because the saved computational cost outweighed the decrease in accuracy (see 4.2.1 for more information).

3.2.4 Sensitivity study

The dynamic validation test is a precise impact test where all parameters have tolerances, height, speed, weight. The tolerances are specified in table 2.1. A study was conducted to assess the impact of the maximum and minimum values within these tolerances on the performance of the FE aPLI models. The objective was to ascertain whether the FE aPLI models results would diverge significantly or remain within acceptable limits under varying conditions. Eight tests were conducted, where for each test only one parameter would be altered from the baseline values. The test matrix can be seen below (0 means no changes will be made to the baseline values from table 2.1. These tests were conducted on both versions of the FE aPLI models.

Table 3.1: Test matrix for sensitivity study.

Test no.	aPLI version	Impact type	parameter change
1	Humanetics	1	All parameters max
2	Humanetics	1	All parameters min
3	Humanetics	2	All parameters max
4	Humanetics	2	All parameters min
5	ATD	1	All parameters max
6	ATD	1	All parameters min
7	ATD	2	All parameters max
8	ATD	2	All parameters min

3.3 Legform to bumper test

Physical impact tests were conducted on a GVTR to gather data and compare it to the signal response of the FE aPLI models in a simulated legform-to-bumper test with an FE representation of the GVTR. The physical test rig comprised foam blocks of varying sizes arranged to imitate a typical vehicle front geometry for correlation investigations. Each block was securely attached to the rig using duct tape.

It should be noted that the physical GVTR and its FE replication were not built during this work but were created previously.
In the FE representation of the GVTR, the foam blocks were affixed to the rig in a manner that wasn't feasible in reality. After completing the physical tests and receiving the results, simulations were conducted using two different duct-taping methods for the foam blocks.

A schematic view of the Humanetics FE aPLI model and the FE GVTR is shown below in Figure 3.9.
A total of eight physical impact tests were conducted at two different heights. The height is the distance between the bottom of the GVTR and the bottom of the aPLI at impact. The first height, referred to as "-40," was 239 mm. The second height, referred to as "-60," was 259 mm. A schematic of the different impact heights is shown in the figure below.

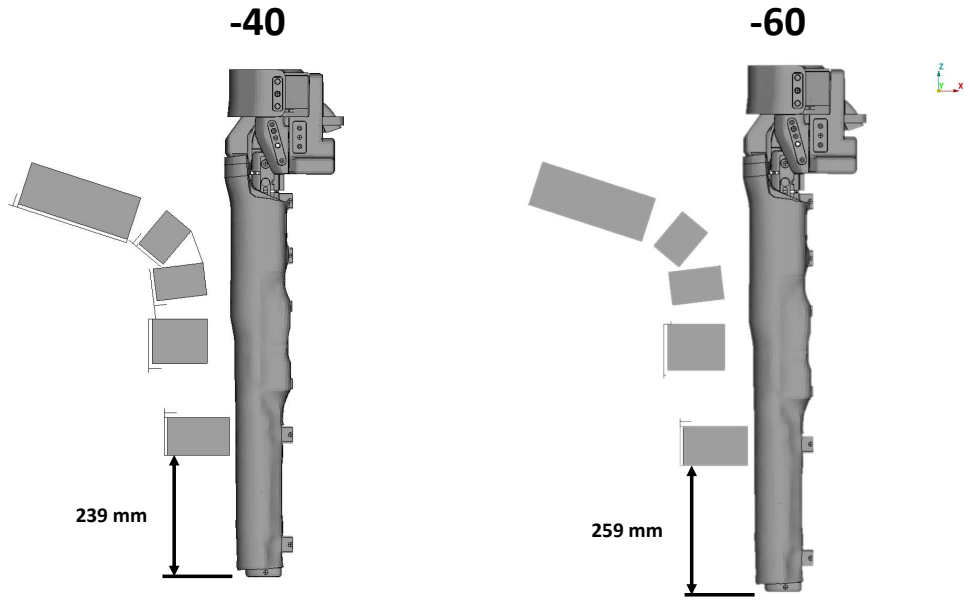

Figure 3.9: Schematic side view of GVTR and the two different test heights.

3.3.1 Variation in the physical impact tests

There was small variation in physical testing for the 8 impact tests conducted, mainly impact height and impact speed. In the table below 3.2 the variance in the 8 physical tests can be seen. Test height is a value given from the positioning of the aPLI in relation to the global coordinate system i.e. the height that the aPLI was intended to strike the GVTR, and the actual impact height is the observed height from high speed cameras used during testing.

Table 3.2: GVTR variance in physical testing.

Test nr	Test height name	Average impact height	Average Impact speed
1 - 4	-40	-231.3 mm	11.1 m/s
5 - 8	-60	-251.3 mm	11.1 m/s

From the results obtained in the physical tests, corridors representing the upper limit, average value and lower limit were constructed for the two different heights. The upper limit of the corridor formed by these curves was determined by generating

a new curve denoted as $y_{upper}(x)$ This curve followed the maximum value among the four curves at each point along the x-axis, expressed mathematically as:

$$y_{upper}(x) = max(f_1(x), f_2(x), f_3(x), f_4(x)) \tag{3.1}$$

The same was done to get a lower limit of a corridor, expressed mathematically as:

$$y_{lower}(x) = min(f_1(x), f_2(x), f_3(x), f_4(x)) \tag{3.2}$$

And to get the average of value of all the curves was calculated as:

$$y_{average}(x) = \frac{f_1(x) + f_2(x) + f_3(x) + f_4(x)}{4} \tag{3.3}$$

3.4 Signal processing

This chapter covers the signal processing performed during the project.

3.4.1 Simulation post processing

All signals were filtered using CFC (Channel Frequency Class) 180 filter according to ISO/TS 20458:2023 to remove noise and distortion. To improve visual clarity during the comparison of signals from physical and simulated tests, it may be necessary to phase-shift certain signals (curves) to align the time of impact.

To ensure robustness in the model, simulations were conducted on various cluster nodes to ensure consistency of the outcome.

3.4.2 Curve shape comparison

To evaluate how well the signal response from simulations compare to physical impact tests the built in compare tool WIFac (Weighted Integrated Factor)(Hovenga et al., 2005) was used in the post processing in META. WIFac provides a result between 0 to 1, where 0 signifies no similarity and 1 signifies a perfect match. The equation can be seen below.

$$crit = 1 - \sqrt{\frac{\int_t max(|f(t)|), |g(t)|) \cdot \left(1 - \frac{max(0, f(t) \cdot g(t))}{max(f(t)^2, g(t)^2)}\right)^2 dt}{\int_t max\Big(|f(t)|, |g(t)|\Big) dt}} \tag{3.4}$$

When comparing the simulation results from the signals to the physical results for each signal, a combined score can be calculated. The combined score was calculated using the Root Mean Square (RMS) addition method to ensure sensitivity to the results of many tests. When calculating the combined score, a weighted factor was used. This factor was determined to be more important for six out of the eight signals. These six signals was Femur up, Femur mid, Femur low, MCL, Tibia up,

and Tibia mid up and were weighted equally at 0.15. The remaining two signals, Tibia mid low and Tibia low, were weighted at 0.05. The RMS formula is shown below.

$$\text{comb} = 1 - \sqrt{\frac{\sum(W \cdot (1 - \text{crit})^2)}{\sum W}} \tag{3.5}$$

3.5 Tuning Humanetics aPLI using Borderline tool and output from physical calibration

When conducting simulations with the FE aPLI models, it is desirable for the results to closely match reality. If there are deviations between the simulation output and physical test results, it is more advantageous if the simulation generates slightly higher values than those observed in physical tests, providing a safety margin. By utilizing output from physical calibration tests as input and incrementally increasing it, it becomes feasible to determine settings for the borderline tool. These settings ensure that the Humanetics FE aPLI model outputs at least a few percentage points higher than the physical aPLI.
The initial tuning were conducted using the honeycomb as the impactor due to the physical calibration tests conducted was with a honeycomb.

4

Results

This chapter will showcase the outcomes of various project stages, starting from the creation and validation of the honeycomb structure, followed by the validation of the FE aPLI models in conjunction with the honeycomb. Subsequently, it will present the results from impact tests with the GVTR.

4.1 Honeycomb validation

To determine whether the FE aPLI models perform according to ISO/TS 20458:2023, the importance of the honeycomb structure's deformation is crucial. Through gradual testing of different types and sizes of elements, improvements in kinematics became evident. Even tough the model with quadrilateral elements had half the number of elements and a faster computational time, it was also observed to have high proportions of hourglass energy. It was observed that triangular elements captured the structure's deformation more closely to the physical counterpart comparing visual deformation from physical validation tests. With a simulated deformation that resembled a physical one, it became possible to begin testing various wall thicknesses to achieve the crush strength specified in ISO/TS 20458:2023. In figure 4.1, the crush curve for the honeycomb structure illustrates its ability to withstand loads up to approximately 16.6 kN before deforming and being crushed. This final itteration of the honeycomb structure had triangular elements with a cell size of 1.2 mm and a wall thickness of 0.007 mm. Experiments where manipulation of the C.O.G were conducted but had no effects on the output results of the FE aPLI models.

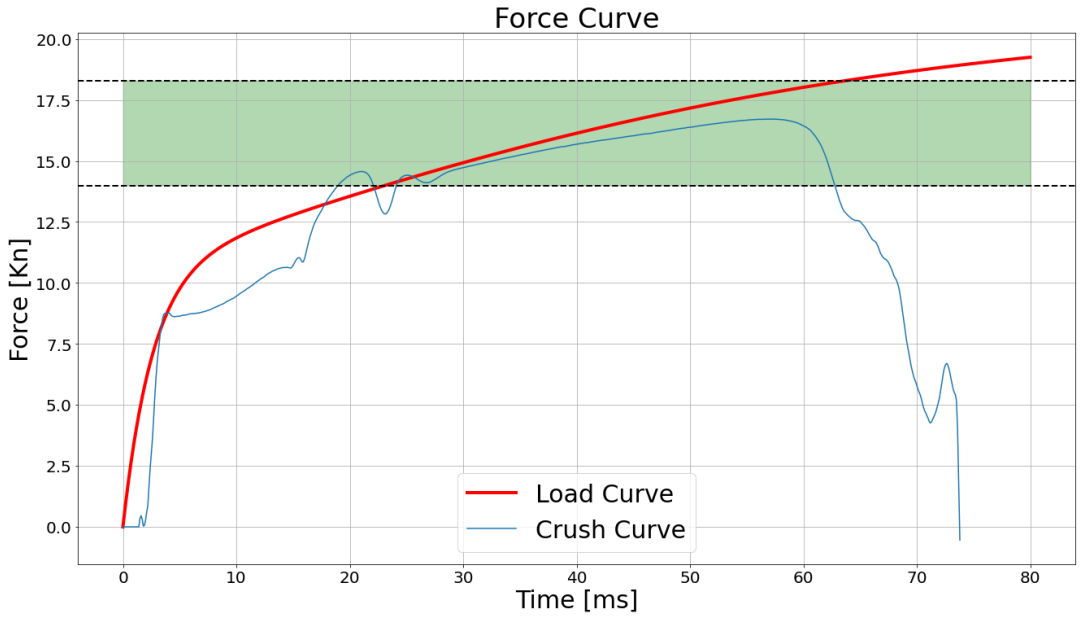

Figure 4.1: The green area in the graph is the accepted limit specified in ISO/TS 20458:2023. The crush curve (blue in figure) is the cross sectional force measured in the honeycomb structure with triangular elements with element size of 1.2 mm and wall thickness of 0.007mm. The red curve is the load profile of how the force is applied on to the sled attached to the honeycomb.

4.2 Simulation results from dynamic validation test

This section deals with the optimazation and calibration of Humanetics FE aPLI model, and comparing the performence to physical aPLI test output. Experiments where manipulation of the C.O.G were conducted but had no effects on the output results of the aPLI and will not be presented.

4.2.1 Optimizing simulation results

The effect of Selective Mass Scaling (SMS) resulted in a reduction in simulation time by a factor of 6.5. Accuracy loss was quantified by comparing the signal response from the FE aPLI models without SMS as the baseline. On average, the mean difference in signal response increased by around 2%. Detailed information on computation time saved with SMS can be found in the tables below. The small difference in signals was deemed acceptable without compromising accuracy, and simulations involving the honeycomb structure continued with SMS.

Table 4.1: Time step reduction using mass scaling for Type 1.

Simulation Type 1	Timesteps	CPU time	Hours	Max Diff
Without mass scaling	1258950	45572	12.7 h	N/a
With mass scaling	102881	6850	1.9 h	3.4%

Table 4.2: Time step reduction using mass scaling for Type 2.

Simulation Type 2	Timesteps	CPU time	Hours	Max Diff
Without mass scaling	1275473	44070	12.2 h	N/a
With mass scaling	102881	6506	1.8 h	6.2%

4.2.2 Calibration of Humanetics FE aPLI model

As explained in Section 3.2.1, two approaches were presented to calibrate the Humanetics FE aPLI model. When efforts were made to calibrate the FE aPLI model, it was revealed that changing one parameter would affect the results of other parameters. For example, decreasing the femur middle parameter would decrease all femur outputs and, in some cases, the ligament elongation as well. Calibrating the FE aPLI model toward the middle of the corridor proved to be more complex than anticipated. Thus, for the calibration version where the FE aPLI model would output values from the middle of the corridor, it was calibrated in the middle of the corridor using the Borderline tool. Simulations were then conducted on both versions of the Humanetics calibration

4.2.3 Evaluation of borderline tool using calibration output from physical validation test

The test values obtained from the physical validation of the aPLI were input into the borderline tool, enabling the assessment of the simulation setup's accuracy. Minor differences in both bending moments and elongations were revealed by the simulation results. The most notable variance between the results obtained from the physical calibration and the simulation was the tendency of the simulation to produce values slightly lower, by a few percentage points, than those fed into the tool.

4.2.3.1 Bending Moment in Femur Type 1 & Type 2

The deviation of femur bending moment in both impact cases was less the 10 percent between the physical and the simulated tests. For Type 1 4.2a, the measured values at the mid and low sections of the femur were higher in the physical test compared to the simulated test, whereas at the upper section, the physical test showed a lower value. While for Type 2 4.3a, it was only at femur mid a higher value was measured during the physical test. At the two other measuring points the simulated test showed higher values.

No distinct trend can be seen when solely analyzing the difference for the femur. In Type 1, one signal was higher in the simulation, whereas in Type 2, signals were higher in the simulation.

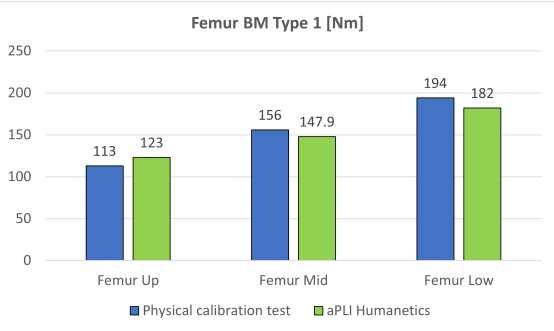

(a) Absolute value of bending moment for physical calibration test (blue) and for the simulation of Humanetics FE aPLI model (green).

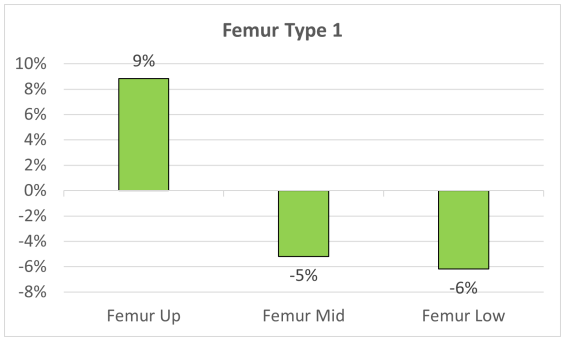

(b) Deviation in percentage between input and output.

Figure 4.2: Type 1: Measured bending moment in the femur for three measuring points. 4.2a and deviation in percentage between input and output4.2b.

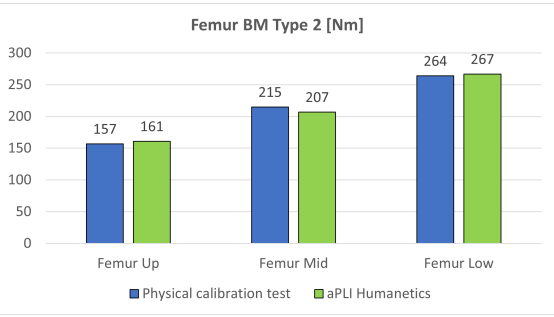

(a) Absolute value of bending moment for physical calibration test (blue) and for the simulation of Humanetics FE aPLI model (green).

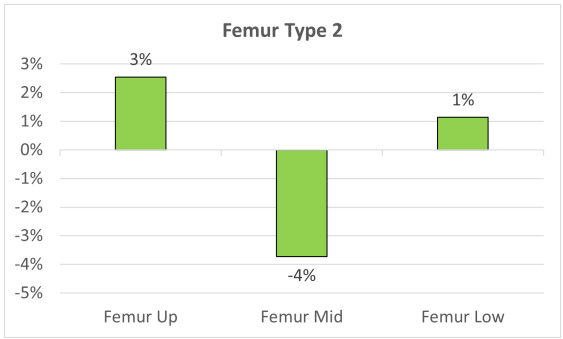

(b) Deviation in percentage between input and output.

Figure 4.3: Type 2: Measured Bending moment in the femur for three measuring points. 4.3a and deviation in percentage between input and output 4.3b.

4.2.3.2 Bending Moment in Tibia Type 1 & Type 2

The overall trend for bending moment in tibia Type 1 4.4a and Type 2 4.5a is that the simulated signal response is a few newtons lower compared to physical test results. This sugests that the Humanetics FE aPLI model is optimistic i.e. it under predicts the signal response. But the deviation between input and output never exceeds 10% in either direction.

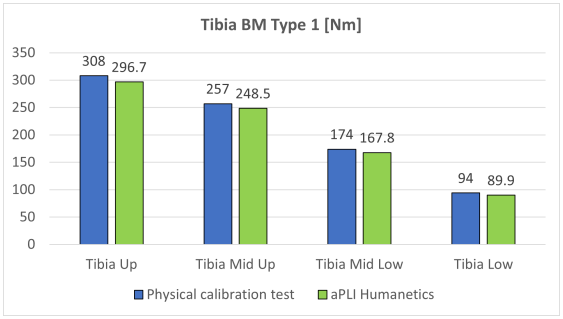

(a) Absolute value of bending moment for physical calibration test (blue) and for the simulation of Humanetics FE aPLI model (green).

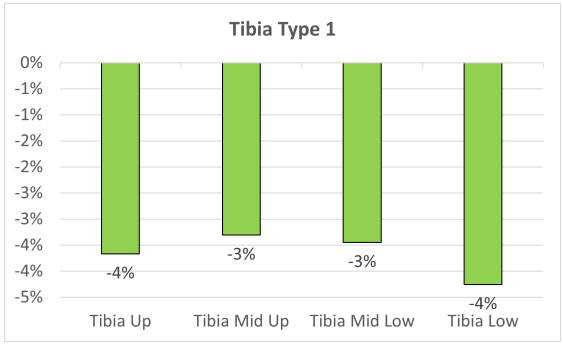

(b) Deviation in percentage between input and output.

Figure 4.4: Type 1: Measured bending moment in the tibia for four measuring points. 4.4a and deviation in percentage between input and output 4.4b.

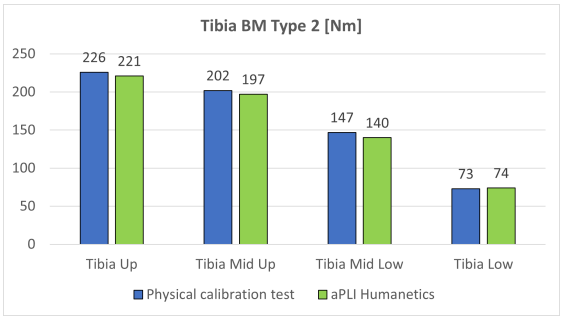

(a) Absolute value of bending moment for physical calibration test (blue) and for the simulation of Humanetics FE aPLI model (green).

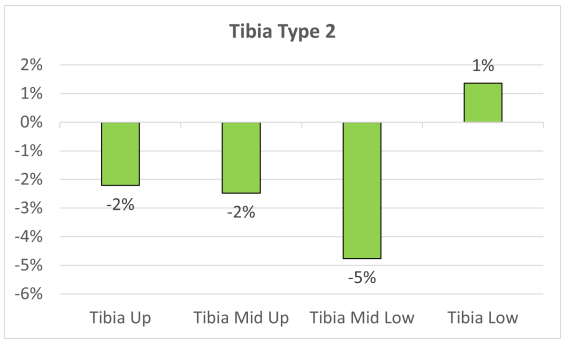

(b) Deviation in percentage between input and output.

Figure 4.5: Type 2: Measured bending moment in the tibia for four measuring points. 4.5a and deviation in percentage between input and output 4.5b.

4.2.3.3 Elongation in Knee Type 1 & Type 2

The trend persists for the knee, with the simulation output consistently lower than the measured values from physical tests used in the borderline tool. However, deviations exceeding 10 percent occur only in Type 1, specifically for the ACL and PCL. In knee assessment, particular attention is placed on the elongation of the MCL since it is the only ligament elongation that matters in Euro NCAP evaluations.

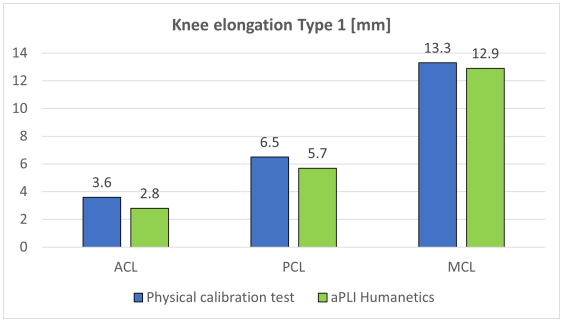

(a) Absolute value of the elongation for the physical calibration (blue) and the simulation of Humanetics FE aPLI model (green), for ACL, PCL, MCL.

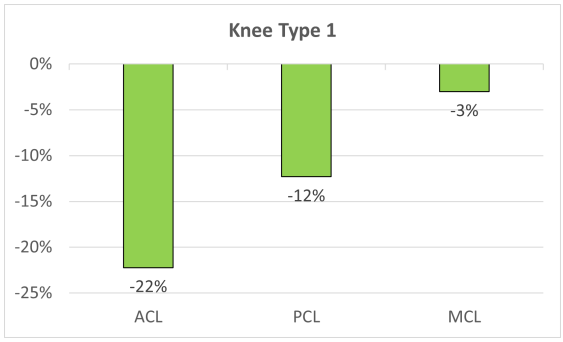

(b) Deviation in percentage between input and output.

Figure 4.6: Type 1: Measured elongation in the knee for ACL, PCL, MCL. 4.6a and deviation in percentage between input and output 4.6b.

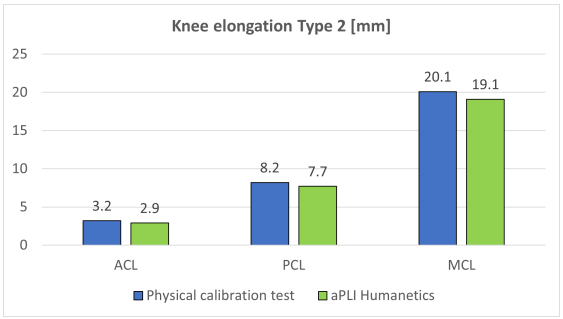

(a) Absolute value of the elongation for the physical calibration (blue) and the simulation of Humanetics FE aPLI model (green), for ACL, PCL, MCL.

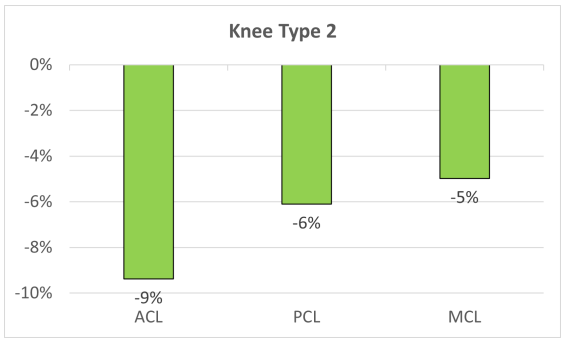

(b) Deviation in percentage between input and output.

Figure 4.7: Type 2: Measured elongation in the knee for ACL, PCL, MCL. 4.7a and deviation in percentage between input and output 4.7b.

4.2.3.4 Summary of borderline tool evaluation

In comparing the simulation results using the honeycomb structure created in the initial part of the project with the outcome from the physical calibration, the general trend suggests the borderline tool tends to be more optimistic. It frequently yields results that are lower than the initially inputted values.

4.2.4 ATDs deviation from physical calibration output using honeycomb

To assess the performance of the FE aPLI model from ATD-models in comparison to Humanetics FE aPLI model, a simulation using an identical setup was conducted for both type 1 and 2, using the same honeycomb structure. The results of these

simulations revealed that the trends observed in the FE aPLI model from ATD-models looked similar to those of Humanetics, but they were much more prominent. Among the 16 input signals examined, ATD-models FE aPLI model surpassed Humanetics in all but one. Figures 4.8 and 4.9 illustrates the disparities between the two FE aPLI models and how much they deviate from the physical calibration output. ATD-models FE aPLI model doesn't allow for tuning the leg with a software tool.

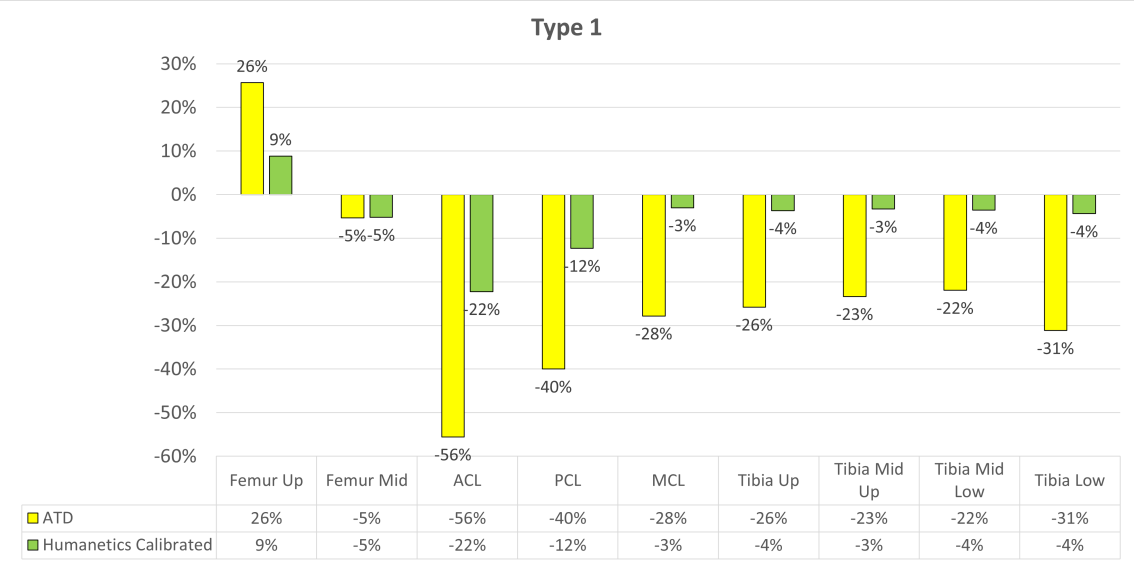

Figure 4.8: Comparison between FE aPLI models from ATD-models and Humanetics and the deviation in percentage from the physical calibration output for Type 1.

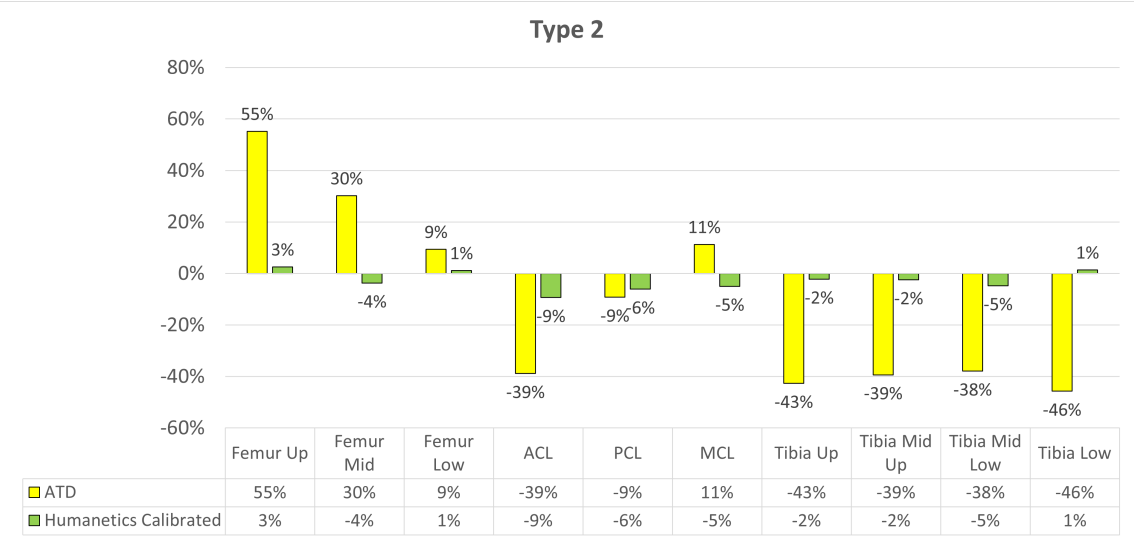

Figure 4.9: Comparison between FE aPLI models from ATD-models and Humanetics and the deviation in percentage from the physical calibration output for Type 2.

4.2.5 Humanetics Baseline deviation from physical calibration output using honeycomb

The final comparison was made using Humanetics with the default settings, referred to as the "Humanetics Baseline." The results showed that the Humanetics Baseline aligned even more closely with the physical validation results than the "Humanetics Calibrated" in most output signals. In several cases, it even overestimated the output compared to the physical test results.

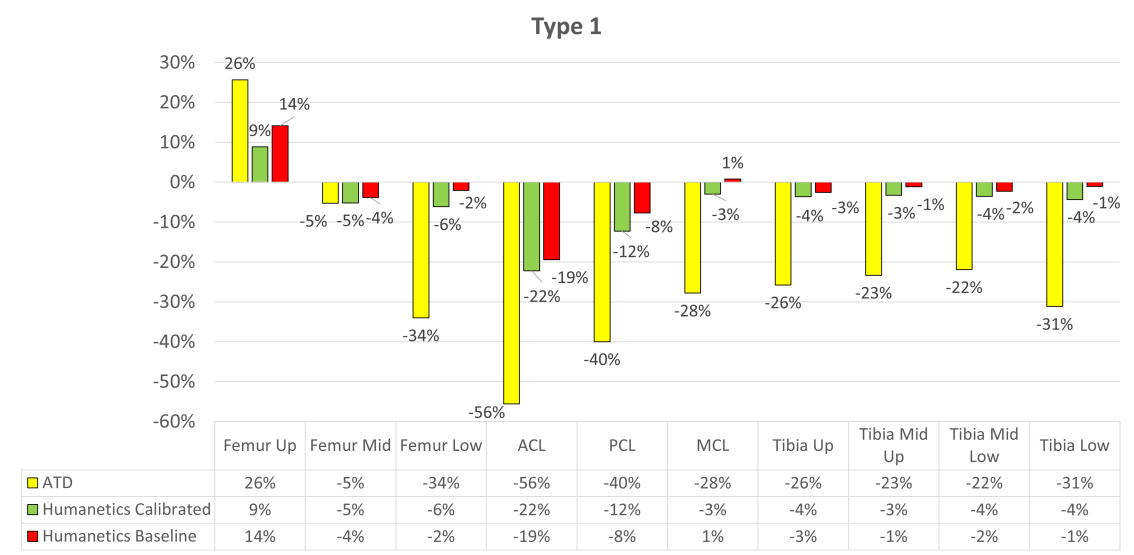

	Femur Up	Femur Mid	Femur Low	ACL	PCL	MCL	Tibia Up	Tibia Mid Up	Tibia Mid Low	Tibia Low
ATD	26%	-5%	-34%	-56%	-40%	-28%	-26%	-23%	-22%	-31%
Humanetics Calibrated	9%	-5%	-6%	-22%	-12%	-3%	-4%	-3%	-4%	-4%
Humanetics Baseline	14%	-4%	-2%	-19%	-8%	1%	-3%	-1%	-2%	-1%

Figure 4.10: Comparison between "ATD-models", "Humanetics Calibrated" and "Humanetics Baseline" and their deviation in percentage from the physical calibration output for Type 1.

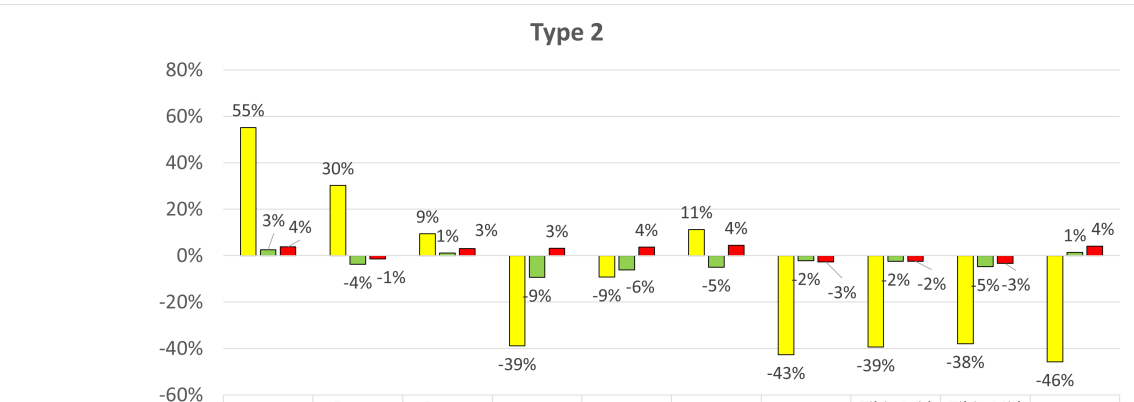

	Femur Up	Femur Mid	Femur Low	ACL	PCL	MCL	Tibia Up	Tibia Mid Up	Tibia Mid Low	Tibia Low
ATD	55%	30%	9%	-39%	-9%	11%	-43%	-39%	-38%	-46%
Humanetics Calibrated	3%	-4%	1%	-9%	-6%	-5%	-2%	-2%	-5%	1%
Humanetics Baseline	4%	-1%	3%	3%	4%	4%	-3%	-2%	-3%	4%

Figure 4.11: Comparison between "ATD-models", "Humanetics Calibrated" and "Humanetics Baseline" and their deviation in percentage from the physical calibration output for Type 2.

4.3 Sensitivity study results

The sensetivity study was conducted to investigate if the extreme values of the ISO standard tolerance in the dynamic validation test would diverge any of the FE aPLI models signals from an acceptable result. Increasing the mass and velocity in the "all parameters maximized" test case increases the kinetic energy in the system compared to the "all parameters minimized" from 478 J to 526 J, this is an increase of 10%. Differences in the signal response from the FE aPLI models in the two test cases should increase and are considered acceptable to change around 10% because of the increase in energy in the system. The results from the sensetivity study showed an increased signal response of 5.5 % (more detailed results can be seen in table A.4, A.5, A.6, A.7 in appendix A). The signals from the FE aPLI models did not diverge towards any unrealistic results thus the impactors can be seen as stable, and further investigations could be continued.

4.4 Impact test against GVTR

4.4.1 Robustness of model

Identical simulations were conducted on different cluster nodes to examine if output results would differ because of an unstable model. The outputs were identical to each other proving a robust model that will have identical results independent of what cluster node is used for simulations.

4.4.2 Physical test results

The peak values of all signals from the physical test are shown below using (3.3).

Table 4.3: Peak values from $y_{average}$ physical test results.

Height	Femur-UP	Femur-MID	Femur-LO	Tibia-UP	Tibia-MID-UP	Tibia-MID-LO	Tibia-LO	MCL
"-40"	341	337	366	229	230	155	72,4	26,6
"-60"	333	339	364	269	220	150	72,7	28,0

4.4.3 Simulation results compared to physical results on GVTR impact test

The graphs below illustrate the difference in peak value between the simulated results and physical impact tests, The values from the physical test can be seen in table 4.3. The horizontal 0% line represents the physical test value, specifically for -40, it is the average value from the four physical tests performed. For -60 height it is done in the same way.

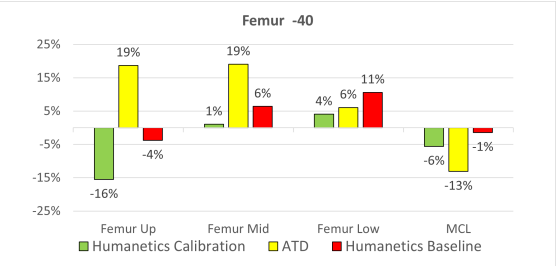

(a) Tibia comparison at height "-40".

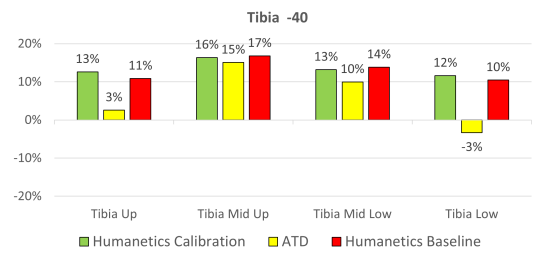

(b) Femur comparison at height "-40".

Figure 4.12: Comparison between HUMANETICS and ATD-models from simulations against GVTR. Results show deviation from physical test data.

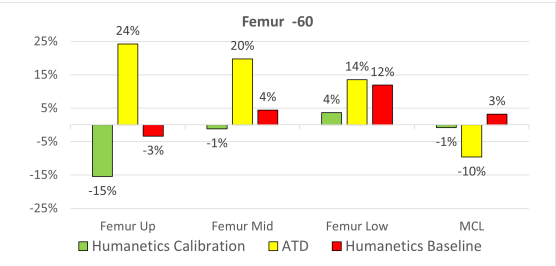

(a) Tibia comparison at height "-60".

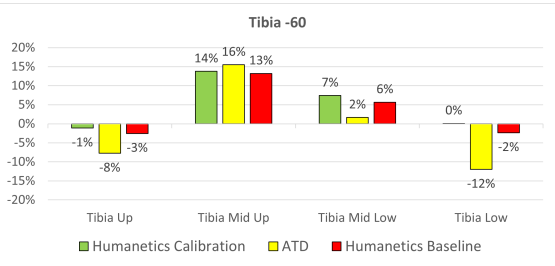

(b) Femur comparison at height "-60".

Figure 4.13: Comparison between HUMANETICS and ATD-models from simulations against GVTR. Results show deviation from physical test data.

4.4.4 Humanetics conservative calibration

A conservative FE model is preferred over an optimistic one that underpredicts impact results. To ensure conservatism across all signal outputs, calibrations were conducted in the borderline tool. These calibrations involved increasing the input parameters by 5% and 10% from the physical calibration.

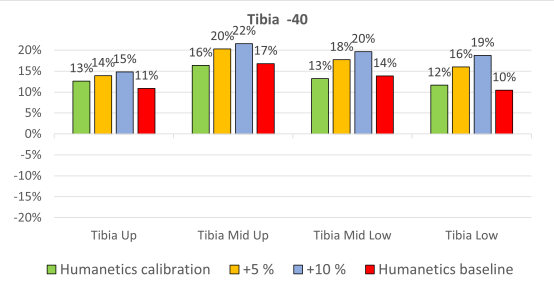

(a) Tibia comparison at height "-40" for Humanetics FE aPLI model.

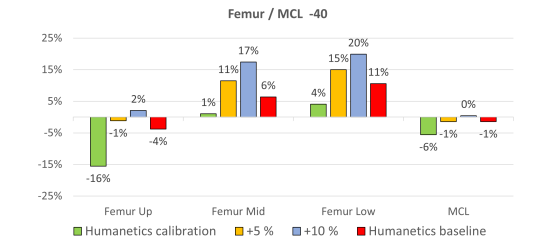

(b) Femur comparison at height "-40" for Humanetics FE aPLI model.

Figure 4.14: Comparison between HUMANETICS baseline calibration and baseline +5% and +10% from simulations against GVTR. Results show deviation from physical test data.

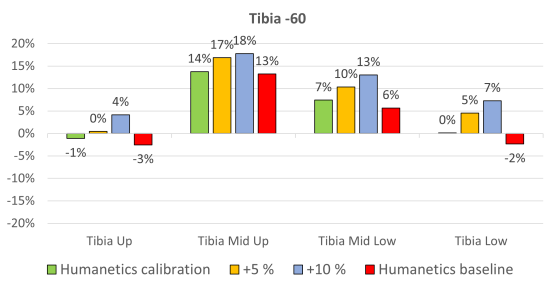

(a) Tibia comparison at height "-60" for Humanetics FE aPLI model.

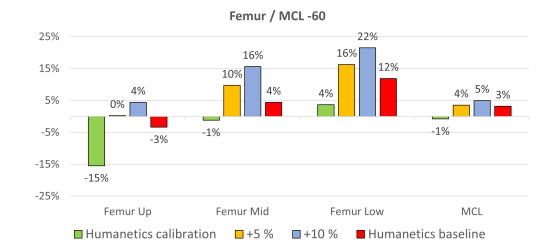

(b) Femur comparison at height "-60" for Humanetics FE aPLI model.

Figure 4.15: Comparison between HUMANETICS baseline calibration and baseline +5% and +10% from simulations against GVTR. Results show deviation from physical test data.

4.4.5 WIFac comparison results

Below here are the results from WIFac comparison. The values displayed in the table represent the degree of alignment, expressed as a percentage, with a baseline curve determined by the average value from the physical tests.

Table 4.4: WIFac results from all signals and how closley they align to the average value from the physical tests.

Signal	Femur-UP	Femur-MID	Femur-LO	Tibia-UP	Tibia-MID-UP	Tibia-MID-LO	Tibia-LO	MCL
ATD -40	78.5%	79.9%	83.8%	82.2%	78.7%	72.1%	63.9%	85.1%
ATD -60	77.7%	79.8%	84.0%	81.8%	77.0%	70.4%	60.5%	81.8%
Humanetics Cal -40	77.8%	82.7%	85.7%	83.1%	82.1%	76.4%	68.9%	82.8%
Humanetics Cal-60	74.8%	81.7%	85.9%	82.7%	80.5%	74.5%	66.2%	80.8%
Humanetics Base -40	82.5%	87.2%	89.4%	86.2%	83.6%	77.6%	71.3%	87.8%
Humanetics Base -60	78%	85.8%	89.8%	85.1%	82.1%	76.7%	69.9%	84.9%

It can be observed in the table below that Humanetics Baseline matches the physical tests the best acording to Wifac calculations.

Table 4.5: Combined scores (3.5) using RMS method with weighted factors.

	ATD	Humanetics Calibration	Humanetics Baseline
Combined Score	78.9%	80.3%	83.5%

4.4.6 Attachment of foam

Since the foam was taped to the GVTR differently than in the simulations, both tape setups were simulated. The test results indicated a difference in results of less than 1%. Detailed variations in results can be observed in the table below.

Table 4.6: Difference between modeled attachments of foam blocks.

Default Values	**Attachment Alt 1**	**Attachment Alt 2**	**Difference**
Femur Upper	323.9 Nm	322.3 Nm	0.49%
Femur Mid	355.7 Nm	353.5 Nm	0.62%
Femur Lower	409.8 Nm	408.7 Nm	0.27%
MCL Elongation	29.14 mm	28.92 mm	0.75%
Tibia Upper	261.8 Nm	262.3 Nm	0.19%
Tibia Mid Upper	248.7 Nm	249 Nm	0.12%
Tibia Mid Lower	157.7 Nm	157.8 Nm	0.06%
Tibia Lower	71.02 Nm	71.02 Nm	0%

4.4.7 Replicating Physical GVTR Tests in Finite Element Environment

The initial setup aimed for consistency across each individual physical test height; however, inherent variation was inevitable. To address this, the corridors based on, maximum, and minimum values from section 4.4 were used to compare physical and simulated results. Replicating the physical tests in the FE environment involved determining the impact speed and height from the physical aPLI through observation using high-speed camera footage. These parameters were then utilized to conduct individual FE simulations, facilitating the analysis of variance between the physical tests and FE tests. Maximum, mean, and minimum curves were computed using equations 3.1, 3.2, 3.3. This process resulted in the creation of corridors, as illustrated in 4.16a and 4.16. Neither of the black lines intersects with each other, nor do the red lines intersect.

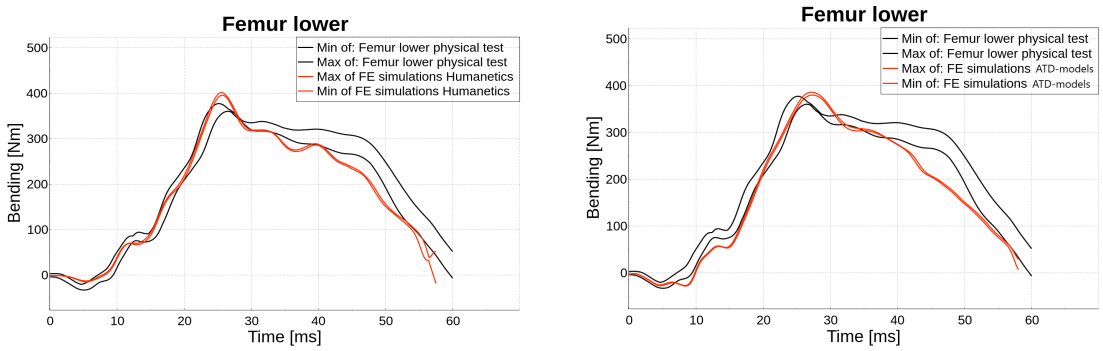

(a) Physical test corridor and simulated test corridor with Humanetics. Neither of the black lines intersects with each other, nor do the red lines intersect.

(b) Physical test corridor and ATD-models corridor. Neither of the black lines intersects with each other, nor do the red lines intersect.

Figure 4.16: Comparison of curve displacement between physical test and FE simulation: Humanetics FE aPLI model versus ATD-models FE aPLI model.

From the figures 4.16a and 4.16, it is obvious that the physical tests have a greater spread of the results than what occurs in the simulated tests for either of the FE aPLI models. The rest of the comparison can be seen at A.1.

5
Discussion

This chapter discusses the results presented in chapter 4.

5.1 Dynamic validation test

To validate the dynamic validation model, results from the latest physical validation of the aPLI was used. For Humanetics aPLI the borderline tool was utilized to calibrate the FE aPLI as the physical aPLI. The results from Humanetics aPLI closely resembled the physical results with a tendency of under performing, ie results from the simulations were a couple percent under what was expected. Despite the results not aligning exactly as the physical tests, it is believed that they are sufficiently close to the specified requirements. The margin of error could stem from differences or defects in the honeycomb structure or the initial boundary conditions that were not exactly the same compared to the one used in the physical tests. It could also be that the sensors in the physical aPLI are calibrated more sensitve then the FE aPLI and thats why the physical values are higher. Much more time could be devoted to further refining the honeycomb structure, but for the purpose of this thesis, the structure performed good enough.

When testing the ATD-models aPLI, no tuning could be performed to match the physical test output. Therefore, outputs from the ATD-models aPLI should remain within the acceptance corridor specified in ISO/TS 20458:2023 (**??**). This was not the case, all results except for the MCL elongation either overshot or under shot the corridor by a fair margin. This reinforced the suspicion that the honeycomb structure was poorly modeled. The sensitivity of the model was tested by altering initial conditions to the extreme values still accepted by the tolerances for the dynamic validation test, i.e changing initial velocity, impact height and sled mass. This hade small changes in the results (<10%) and ATD-models aPLI did not get closer to outputting results within the corridor.

5.2 General Vehicle Test Rig impact simulations

This section of the discussion focuses on the comparison of data between the physical test performed on the GVTR and on the simulations made with the aPLI from the two different developers.

5.2.1 Results discussion

Looking at the results in Section 4.4.3, both impactors overshoot and undershoot the desired signals from physical test data. The data is compared to the average value from all the physical tests. The Humanetics aPLI is closer to the peak values of the physical aPLI results compared to ATD-models aPLI in 11 out of 16 signals. If it's desirable to have a conservative model and overshooting is better than undershooting, then all results that are under the desired value are worse than overshooting by any percentage, making the Humanetics model better in 9 out of 16 signals.

The Humanetics aPLI delivers results that are marginally closer to the physical results, probably because it is calibrated towards the physical aPLI. In this case, it has an advantage over ATD-models aPLI. However, in a business case scenario where simulations are conducted on a vehicle up to two years before physical tests, the calibration of the aPLI may not be known beforehand. Knowing how conservative or optimistic the FE aPLI is compared to the physical aPLI is not possible. We believe that a conservative model is better, guaranteeing no surprises during physical tests.

When simulating impacts between vehicles and impactors, it is important that both models are well-correlated, meaning that the contact and material modeling are correct and realistic. This thesis is limited to using the contact modeling called automatic surface-to-surface in LS-Dyna. This might be one of the reasons why the correlation between physical and virtual tests differs. The same applies to the material modeling of the GVTR foam. Further investigation can be done in this area to attain better correlation between simulation and reality.

5.2.2 Tighter spread

A comparison of each individual FE result against the results from the physical tests was conducted to visually observe how the output curves from simulations moved in relation to curves from the physical tests. The physical tests exhibited a wider spread, as demonstrated in figures 4.16a and 4.16, where it can be seen that the generated corridor is wider than the one produced by the FE simulations. In the FE simulations, the exact parameters obtained from each physical test were used in the model and this resulted in a much tighter spread. Since the simulations are based on mathematical models and calculations, they are not susceptible to external factors like the physical tests.

5.2.3 WIFac

Many of the signals within the borderline tool from Humanetics are dependent on each other, meaning adjustments to one signal may impact the others, making it a challange to precisely anticipate how each signal will react to individual adjustments. To assess simulation accuracy, the built-in function to compare curves, WIFac in Meta, was utilized after each simulation run. This function compares simulated

curves against curves derived from physical test data, expressing the comparison in percentages.

Using default values from Humanetics as the baseline in the simulations, resulted in higher percentage similarity with physical test curves, even though that the simulated curves exceed the physical test curves, yielding higher maximum values. This trade-off was weighed against the adjusted curves, which exhibited a lower percentage similarity with the physical test curves but approached the maximum values more closely.

It is desirable to have a model that is conservative in the sense that simulations tend to yield higher values than the actual physical test models. Therefore, if the simulated curve exceeds the physical test curve, it can be advantageous. In Euro NCAP assessments, they focus on the highest measured values from the physical tests they perform. That is why it is important with an accurate and predictable FE representation.

When simulating legform to bumper impact tests, it is better to have output signals accurately predict the maximum value of the physical signal rather than scoring a high WIFac score. This is because the maximum signal response is crucial for the Euro NCAP rating.

5.2.4 Tuning Humanetics FE representation of aPLI

Initially, when comparing the curves from the Humanetics FE aPLI using default values, it was observed that it had a higher average percentage of likeness to the average physical test curve than what was obtained after tuning. Our objective in tuning the FE aPLI was to align the simulated curve's shape more closely with that of the physical test curve. An interesting observation was that the closer the simulated curve approached the shape of the physical curve, the more it diverged according to the WIFac method.

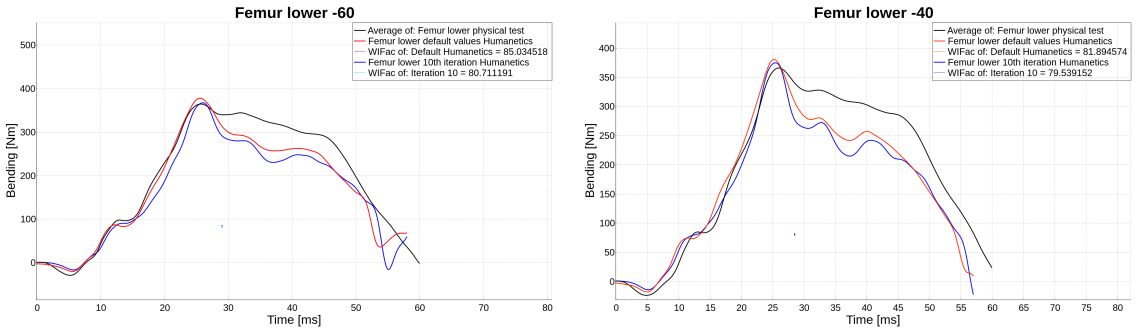

(a) WIFac femur lower on test height -60 **(b)** WIFac femur lower on test height -40

Figure 5.1: WIFac comparison, physical test against both default values and 10th iteration. (Only Humanetics aPLI)

The most notable difference observed when comparing the curve from the FE aPLI using default values to the physical curve using the average value from each test height, was that it closely aligned with the physical curve initially before it overshot and then rapidly declined.

The blue curve in figure 5.1 representing the humanetics FE aPLI with tuned values exhibited a shape that closely aligned with the physical curve initially. It never overshot as high as the FE aPLI with default values and were much more closely to the same maximum values as the physical test curve. The downside with the tuned FE aPLI was that it was consistently further below both the physical curve and the curve with default values.

In summary, tuning the Humanetics FE aPLI can result in a maximum value closer to that of the physical aPLI, but the overall curve may deviate further from the physical test curve. If instead using default values for the FE aPLI, it yields a curve that aligns more closely with the physical test curve, but with a maximum value exceeding the physical maximum value.

5.2.5 Change of calibration over time

During a later phase of the project, while compiling data and information for the report, data from previous calibrations of the physical aPLI were also reviewed. It was observed that between the two most recent calibration tests of the physical aPLI, the calibration had changed over time. Some sensors appeared to have become less sensitive, while others had become more sensitive. This highlights the importance of having recent data from a physical calibration test.

Table 5.1: Change of calibration over time for impact Type 1 in the dynamic validation test. Some sensors have become less sensitvie and some have become more sensitive between calibrations.

Measurement Type 1	2023-04-17	2023-11-30	Change [%]
Femur Upper [Nm]	122.11	113.1	-7.4% ↓
Femur Mid [Nm]	152.41	155.6	2.1% ↑
Femur Lower [Nm]	202.60	194.2	-4.1% ↓
ACL [mm]	5.82	3.6	-38.1% ↓
PCL [mm]	6.94	6.5	-6.3% ↓
MCL [mm]	14.68	13.3	-9.4% ↓
Tibia Upper [Nm]	302.94	307.9	1.6% ↑
Tibia Mid Upper [Nm]	252.93	257.2	1.7% ↑
Tibia Mid Lower [Nm]	166.85	173.8	4.1% ↑
Tibia Lower [Nm]	97.52	94.2	-3.4% ↓

Table 5.2: Change of calibration over time for impact Type 2 in the dynamic validation test.

Measurement Type 2	2023-04-17	2023-11-30	Change [%]
Femur Upper [Nm]	153.21	156.8	2.3% ↑
Femur Mid [Nm]	210.91	214.9	1.9% ↑
Femur Lower [Nm]	271.96	263.9	-3% ↓
ACL [mm]	3.37	3.2	-5% ↓
PCL [mm]	8.77	8.2	-6.5% ↓
MCL [mm]	22.00	20.9	-5% ↓
Tibia Upper [Nm]	217.39	225.5	3.7% ↑
Tibia Mid Upper [Nm]	193.94	202.3	4.3% ↑
Tibia Mid Lower [Nm]	137.50	146.7	6.7% ↑
Tibia Lower [Nm]	68.04	73.3	7.7% ↑

5.2.6 Future studies

More time can be spent on enhancing the honeycomb structure, thereby reducing its margin of error within the test setup, while simultaneously reproducing the tests in a FE environment in combination with new physical tests could lead to a better correlated honeycomb and better knowledge about the spread from the honeycomb structure.

Impact simulations on the gvtr rig at an angle of +30 and -30 were conducted but we didnt have time to conduct the physical impact tests, this angled impact simulates striking the vehicle at the outer edges of the front and could be a good suplimentary result comparing to physical impact tests.

It could be seen in the high speed videos that the GVTR moved a couple millimeters in the impact, investigating how much of an effect this could have on the output from the simulations could be of intrest.

Exact hur skummets material påverkar resultaten har vi inte undersökt Creating new material parameters for the foam used in the GVTR could further investigate why the physical results differ from the simulated results.

Exact hur kontakt setupen påverkar resultaten har vi inte undersökt Further investigations of contact modeling types could be done to determine which type aligns best with physical test results.

Gather more data from physical aPLI by performing additional GVTR tests to evaluate the spread from a larger dataset.

6
Conclusion

This thesis compared two FE-models of the advanced Pedestrian Legform Impactor, one from Humanetics and the other from ATD-models. These models were evaluated against a physical unit in two types of dynamic tests. The Humanetics FE aPLI provided performance much closer to the physical aPLI in the dynamic validation simulations and performed more consistently in simulations against the GVTR. In contrast, the FE aPLI from ATD-models showed larger deviations from acceptable results.

Furthermore, significant variations were observed in several injury-predicting parameters during the dynamic validation test. We believe these variations were due to imperfections in our honeycomb modeling. Unlike the Humanetics aPLI, the ATD-models aPLI showed significant deviations from the acceptable signal response.

In the sensitivity study, both aPLIs appeared robust. However, the ligament signal response in the ATD-models showed slight deviations compared to other signals, suggesting that the Humanetics aPLI is marginally more robust.

Testing the physical leg against a GVTR revealed a spread of around 5%, likely due to the sensitivity and repeatability of the physical leg. To account for this and ensure a reliable margin of error, it is preferable to use a conservative model when simulating with the aPLI. Such a model should overestimate or remain at the upper limit of the corridor compared to physical test results.

The results from GVTR simulations were mixed, with both aPLIs over- and under-predicting signal responses. Consequently, no definitive better choice emerged from these simulations.

The borderline tool comes with both advantages and disadvantages. One advantage is that it allows for tuning of the leg retroactive according to physical calibration tests. It could also be used with the default settings without any changes. One disadvantage with it is that it can be time-consuming and require thorough and systematic adjustments.
Considering all the results from this project, we recommend the Humanetics aPLI. Nonetheless, further investigation into the material parameters for the GVTR and contact modeling is necessary to improve the correlation of the FE aPLIs. Additionally, more work by the aPLI developers is needed to capture the impactor's complexity accurately.

Bibliography

[1] Belytschko, T., Liu, W.K., Moran, B., Elkhodary, K.I., (2014): Nonlinear Finite Elements for Continua and Structures, Second Edition, ISBN: 978-1-118-63270-3

[2] E.G. Janssen, (1996): EEVC TEST METHODS TO EVALUATE PEDESTRIAN PROTECTION AFFORDED BY PASSENGERS CARS TNO, Paper Number 96-S7-W-17, https://www.eevc.net/EEVC/EN/Past/WG10/Pedestian-Protection.pdf?__blob=publicationFile&v=2

[3] Isshiki, T., Konosu, A., Takahashi, Y.,(2016): Development and Evaluation of the Advanced Pedestrian Legform Impactor Prototype which can be Applicable to All Types of Vehicles Regardless of Bumper Height - Part 1: Finite Element Model - https://www.ircobi.org/wordpress/downloads/irc16/pdf-files/98a.pdf

[4] Han, Y.H., Lee, I.H., Lee, W.R,. (2018) DEVELOPMENT OF A FLEX-PLI SYSTEM MODEL AND INVESTIGATIONS OF INJURY, https://ep.liu.se/ecp/148/007/ecp18148007.pdf

[5] Svenska institutet för standarder, (2024), ISO/TS 20458:2023, edition 1

[6] Autoliv, (2023), RE: Docket No. NHTSA-2030-0020 New Car Assessment Program Request for Comment, https://downloads.regulations.gov/NHTSA-2023-0020-2723/attachment_1.pdf, Accessed February 18, 2024.

[7] Asgari. M., Keyvanian. Sh.S, (2019): Crash Injury Analysis of Knee Joint Considering Pedestrian Safety. J Biomed Phys Eng. ;9(5):569-578. doi: 10.31661/jbpe.v0i0.424. PMID: 31750271; PMCID: PMC6820024, https://www.ncbi.nlm.nih.gov/pmc/articles/PMC6820024/

[8] Euro NCAP, (2024), VULNERABLE ROAD USER TESTING PROTOCOL, https://www.euroncap.com/media/79878/euro-ncap-vru-testing-protocol-v91.pdf, Accessed Mars 8, 2024.

[9] Euro NCAP, (2023), ASSESSMENT PROTOCOL – VULNERABLE ROAD USER PROTECTION, https://www.euroncap.com/media/79885/euro-ncap-assessment-protocol-vru-v114.pdf Accessed Mars 8, 2024.

[10] Humanetics, (2024), Products, https://www.humaneticsgroup.com/products, Accessed April 11, 2024.

[11] Humanetics, (2024), aPLI FE, https://www.humaneticsgroup.com/products/virtual-models/pedestrian-atd-virtual-models/apli-fe/apli-borderline-fe, Accessed April 11, 2024.

[12] ATD-models, (2024), Introduction, http://www.atd-models.com/011_en_company_introduction.html, Accessed April 11, 2024.

[13] Cellbond, (2024), About, https://www.cellbond.com/about/, Accessed April 11, 2024.

[14] Euro NCAP. (2023): How to read the stars, https://www.euroncap.com/en/about-euro-ncap/how-to-read-the-stars/Accessed April 20, 2024.

[15] World Health Organization. (2023): Global status report on road safety, https://iris.who.int/bitstream/handle/10665/375016/9789240086517-eng.pdf?sequence=1

[16] Stewart, T. (2023, April). Overview of motor vehicle traffic crashes in 2021 (Report No. DOT HS 813 435). National Highway Traffic Safety Administration, https://crashstats.nhtsa.dot.gov/Api/Public/ViewPublication/813435

[17] National Center for Statistics and Analysis. (2022, October). Traffic safety facts 2020: A compilation of motor vehicle crash data (Report No. DOT HS 813 375). National Highway Traffic Safety Administration, https://crashstats.nhtsa.dot.gov/Api/Public/Publication/813375

[18] P. E. Hovenga, H. H. Spit, M. Uijldert, A. M. Dalenoort (2005): Improved Prediction of Hybrid-III Injury Values Using Advanced Multibody Techniques and Objective Rating, https://www.sae.org/publications/technical-papers/content/2005-01-1307/

[19] Euro NCAP. (2021): Assessment protocol - Overall rating Version 9.1.1, https://cdn.euroncap.com/media/67890/euro-ncap-assessment-protocol-overall-rating-v911.pdf, Accessed May 3, 2024.

[20] Euro NCAP. (2024): Vehicle Safety - Glossary (v), https://www.euroncap.com/en/car-safety/glossary/

A

Appendix 1

Table A.1: Certification corridors for Inverse Type 1 and the measured values from the physical test

Measurement	Specification	Measurement
Femur Moment Upper	101 - 134 Nm	113.1 Nm
Femur Moment Mid	133 - 178 Nm	155.6 Nm
Femur Moment Lower	162 - 208 Nm	194.2 Nm
ACL Elongation	3 - 4 mm	3.6 mm
PCL Elongation	6 - 8 mm	6.5 mm
MCL Elongation	12 - 16 mm	13.3 mm
Tibia Moment Upper	291 - 334 Nm	307.9 Nm
Tibia Moment Mid Upper	238 - 272 Nm	257.2 Nm
Tibia Moment Mid Lower	160 - 193 Nm	173.8 Nm
Tibia Moment Lower	92 - 116 Nm	94.2 Nm

Table A.2: Certification corridors for Inverse Type 2 and the measured values from the physical test

Measurement	Specification	Measurement
Femur Moment Upper	147 - 190 Nm	156.8 Nm
Femur Moment Mid	189 - 238 Nm	214.9 Nm
Femur Moment Lower	233 - 293 Nm	263.9 Nm
ACL Elongation	3 - 4 mm	3.2 mm
PCL Elongation	8 - 10 mm	8.2 mm
MCL Elongation	20 - 24 mm	20.9 mm
Tibia Moment Upper	206 - 251 Nm	225.5 Nm
Tibia Moment Mid Upper	182 - 228 Nm	202.3 Nm
Tibia Moment Mid Lower	132 - 164 Nm	146.7 Nm
Tibia Moment Lower	63 - 83 Nm	73.3 Nm

Table A.3: The change of the certification corridors

Measurement	**Inverse Type 1**		**Inverse Type 2**	
	From 2021	**From 2024**	From 2021	**From 2024**
Femur Upper	101-134 Nm	**103-136 Nm**	147-190 Nm	**145-193 Nm**
Femur Mid	133-178 Nm	**135-182 Nm**	189-238 Nm	**190-243 Nm**
Femur Lower	162-208 Nm	**165-213 Nm**	233-293 Nm	**234-300 Nm**
ACL Elongation	3-4 mm	**3.2-4 mm**	3-4 mm	**2.8-4 mm**
PCL Elongation	6-8 mm	**5.7-7.6 mm**	8-10 mm	**7.8-9.7 mm**
MCL Elongation	12-16 mm	**12.1-16.5 mm**	20-24 mm	**20.3-24.4 mm**
Tibia Upper	291-334 Nm	**299-339 Nm**	206-251 Nm	**211-249 Nm**
Tibia Mid Upper	238-272 Nm	**245-278 Nm**	182-228 Nm	**187-231 Nm**
Tibia Mid Lower	160-193 Nm	**163-194 Nm**	132-164 Nm	**134-163 Nm**
Tibia Lower	92-116 Nm	**92-115 Nm**	63-83 Nm	**65-83 Nm**

A.0.1 Test height -40 corridors

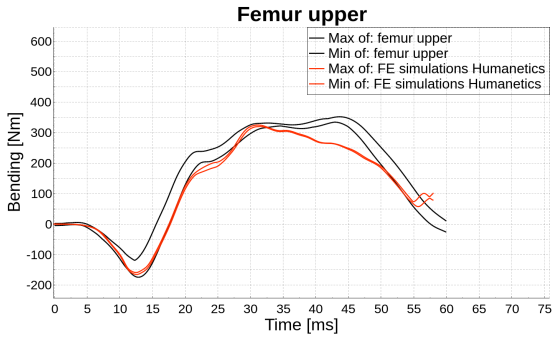

(a) Humanetics

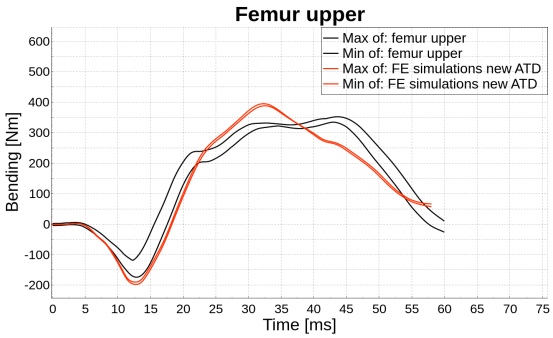

(b) ATD-models

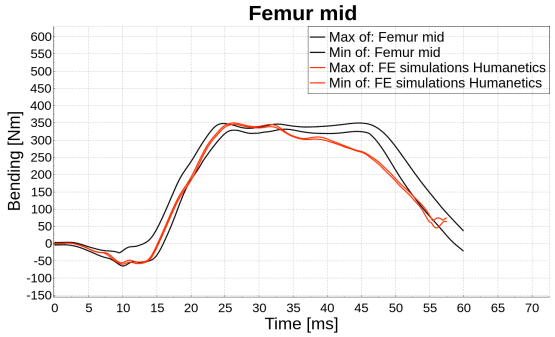

(c) Humanetics

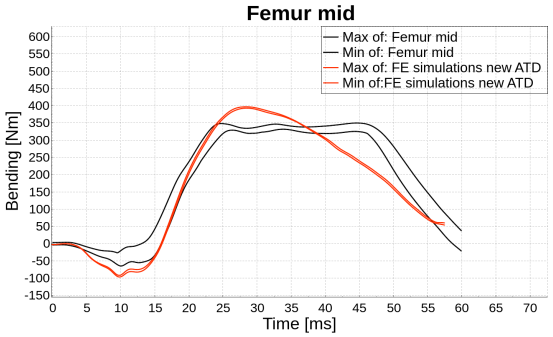

(d) ATD-models

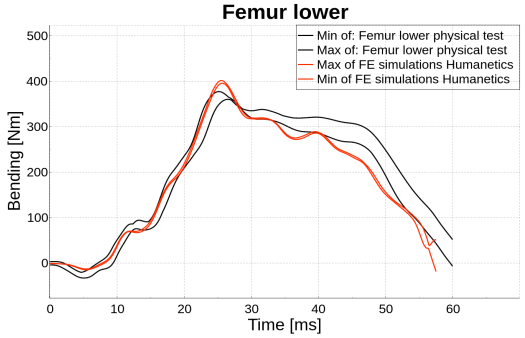

(e) Humanetics

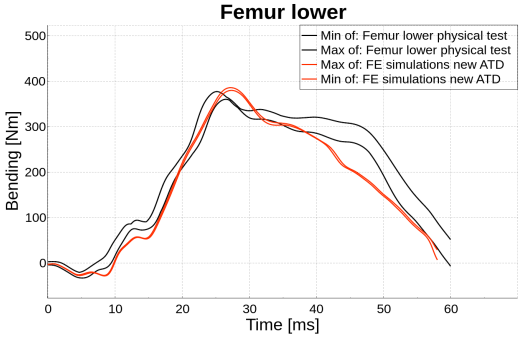

(f) ATD-models

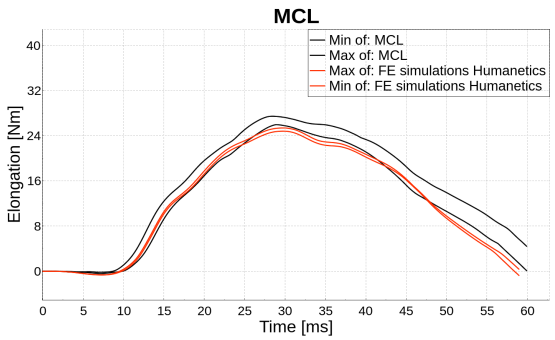

(g) Humanetics

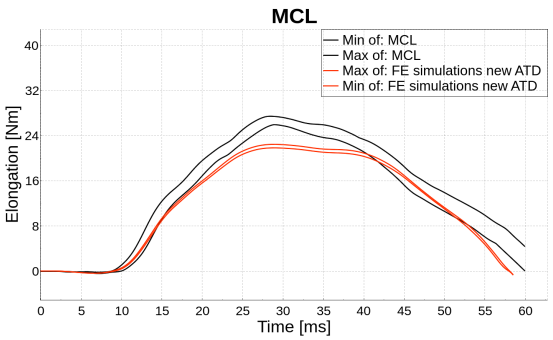

(h) ATD-models

Figure A.1: Physical test corridor vs FE simulations corridor Femur upper, -40

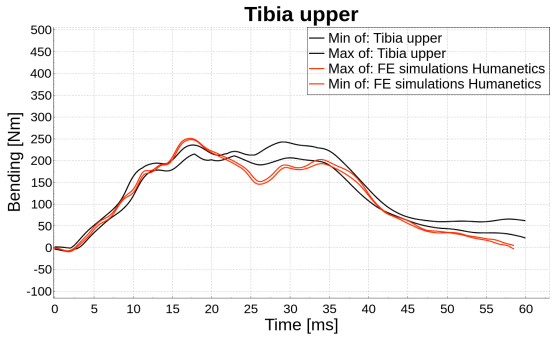

(i) Humanetics

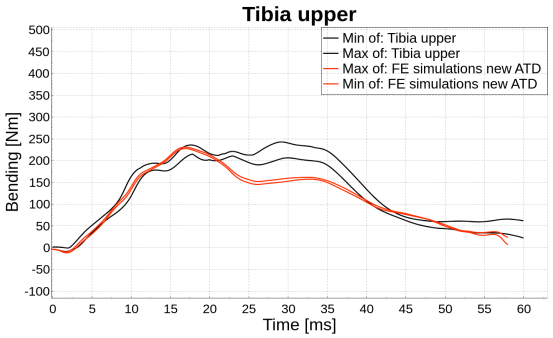

(j) ATD-models

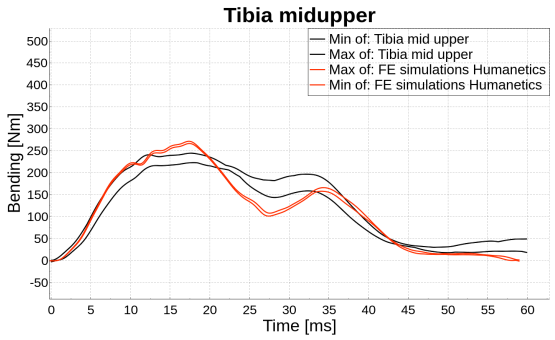

(k) Humanetics

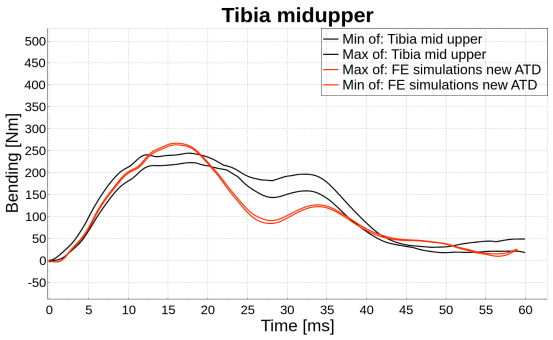

(l) ATD-models

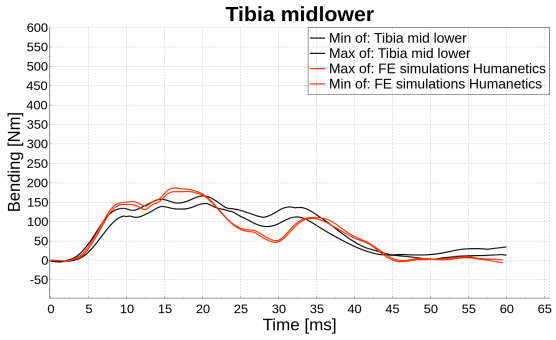

(m) Humanetics

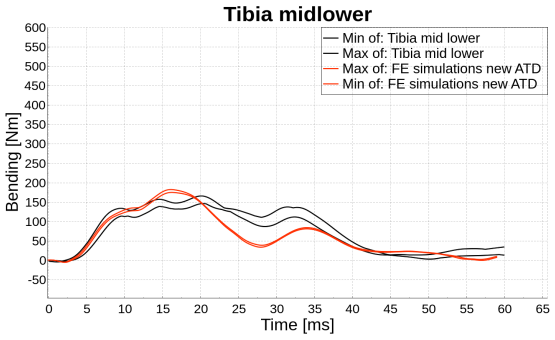

(n) ATD-models

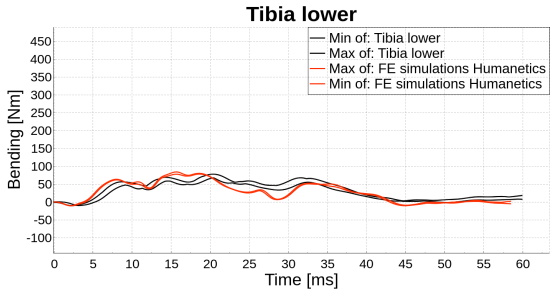

(o) Humanetics

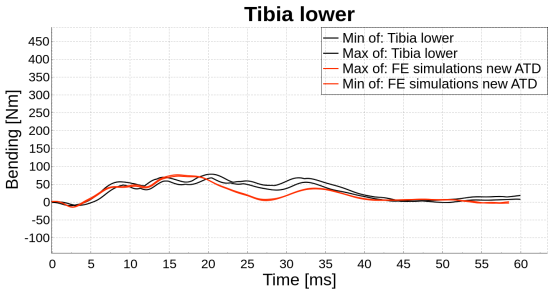

(p) ATD-models

Figure A.1: Physical test corridor vs FE simulations corridor Femur upper, -40

A.0.2 Test height -60 corridors

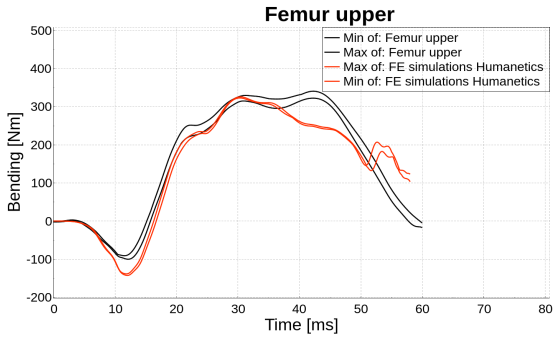

(a) Humanetics

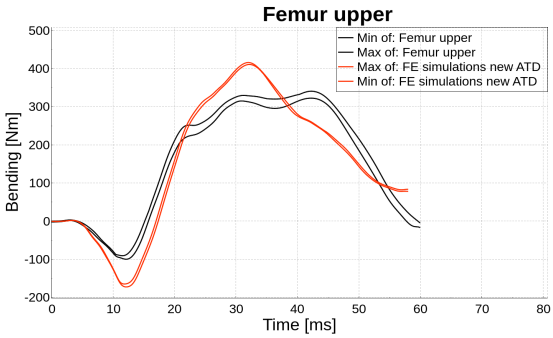

(b) ATD-models

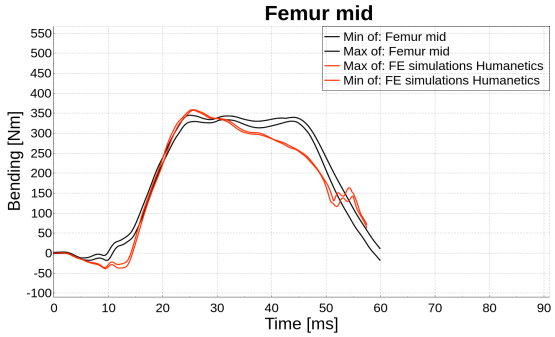

(c) Humanetics

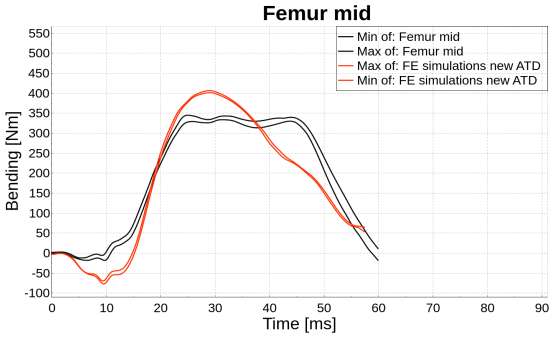

(d) ATD-models

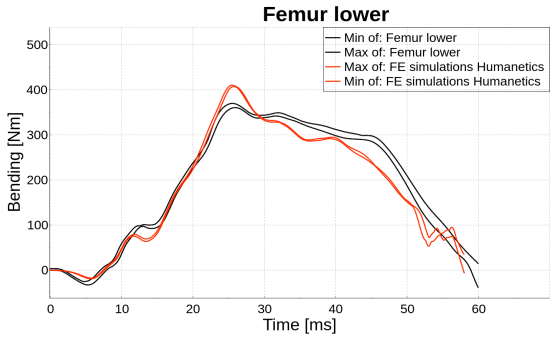

(e) Humanetics

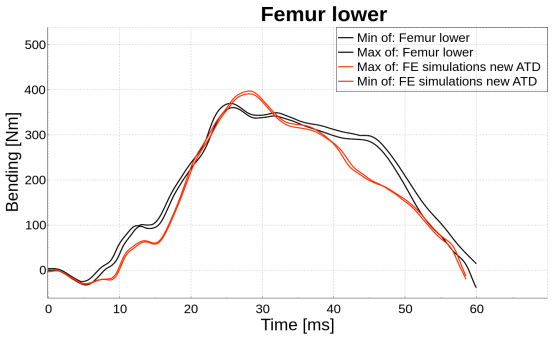

(f) ATD-models

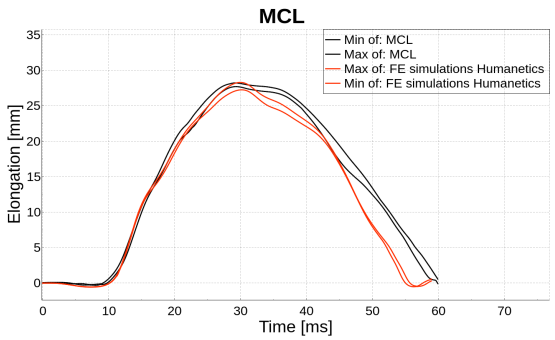

(g) Humanetics

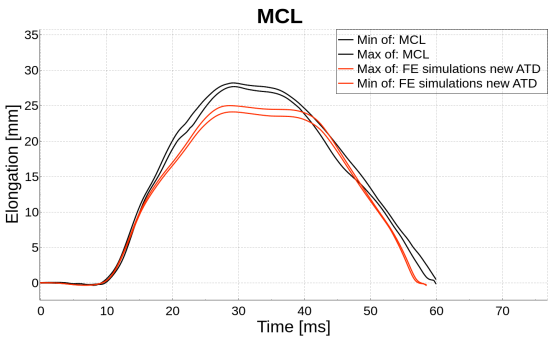

(h) ATD-models

Figure A.2: Physical test corridor vs FE simulations corridor Femur upper, -60

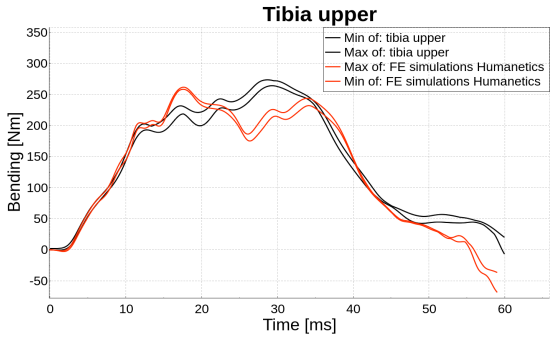

(i) Humanetics

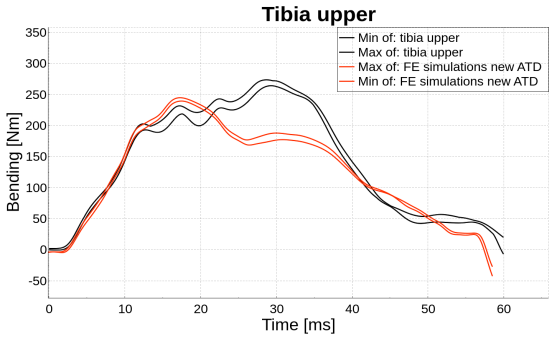

(j) ATD-models

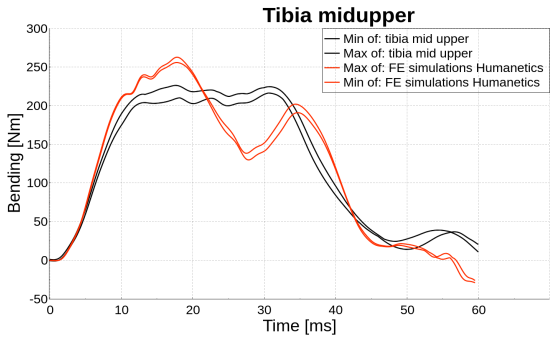

(k) Humanetics

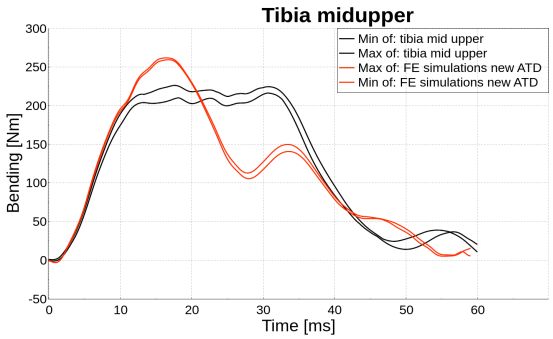

(l) ATD-models

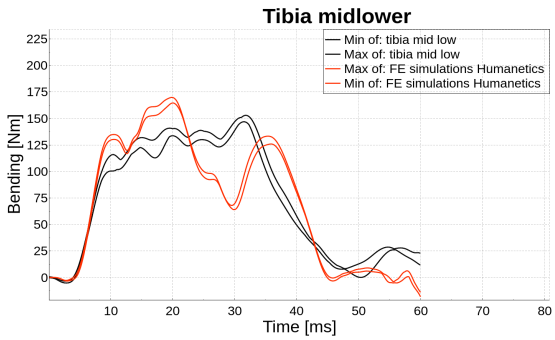

(m) Humanetics

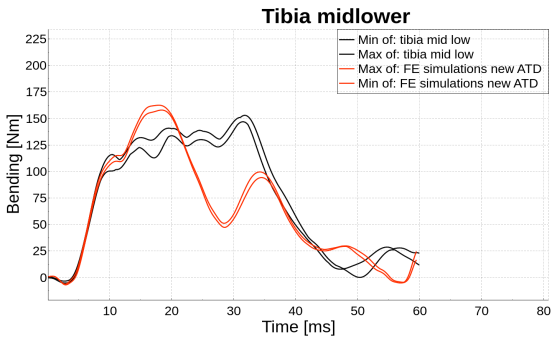

(n) ATD-models

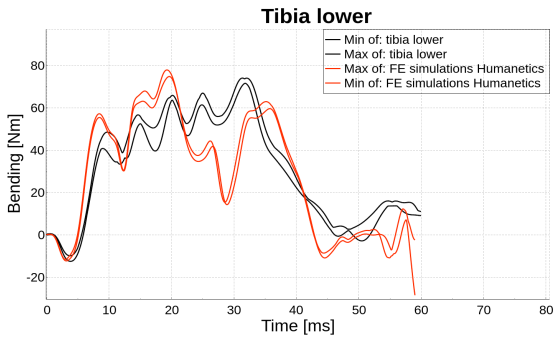

(o) Humanetics

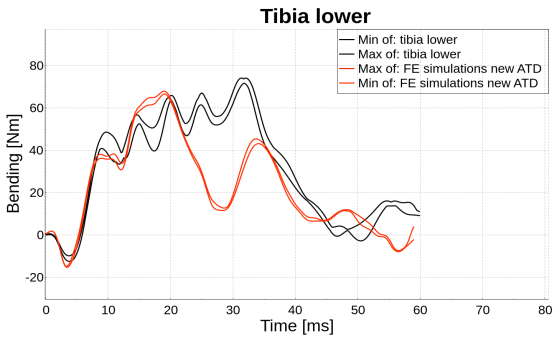

(p) ATD-models

Figure A.2: Physical test corridor vs FE simulations corridor Femur upper, -60

A.0.3 Sensitivity study

Table A.4: Sensitivity study type 1 ATD-models max vs min results

	fem up	fem mid	fem low	tibia up	tibia mid up	tibia mid lo	tibia lo	mcl	pcl	acl	average diff
max [nm]	145.5	150.6	131.6	230.8	196.7	135	64.96	10.14	4.09	1.65	
min [nm]	137.9	144	124.5	222.9	192.9	133.4	62.65	8.95	3.6	1.46	
diff	106%	105%	106%	104%	102%	101%	104%	113%	114%	113%	107%

Table A.5: Sensitivity study type 2 ATD-models max vs min results

	fem up	fem mid	fem low	tibia up	tibia mid up	tibia mid lo	tibia lo	mcl	pcl	acl	average diff
max [nm]	175.5	207.3	218.7	176.4	157.9	109.6	50.3	15.2	6.0	2.3	
min [nm]	168.1	194.8	204.7	171	150.3	104.1	48.8	14.3	5.7	2.1	
diff	104%	106%	107%	103%	105%	105%	103%	106%	107%	107%	105%

Table A.6: Sensitivity study type 1 Humanetics max vs min results

	fem up	fem mid	fem low	tibia up	tibia mid up	tibia mid lo	tibia lo	mcl	pcl	acl	average diff
max [nm]	133	153.6	195.5	303.7	253.4	164.3	91.3	13.7	6.1	2.9	
min [nm]	126.3	147.8	185.8	290.7	245.7	164.2	88.9	13.1	5.8	2.8	
diff	105%	104%	105%	104%	103%	100%	103%	105%	104%	105%	104%

Table A.7: Sensitivity study type 2 Humanetics max vs min results

	fem up	fem mid	fem low	tibia up	tibia mid up	tibia mid lo	tibia lo	mcl	pcl	acl	average diff
max [nm]	167.3	216.8	281.9	222.4	199.2	143.5	76.14	21.6	8.8	3.4	
min [nm]	159.8	206.3	263.8	214.2	190.3	134.8	70.77	20.3	8.2	3.2	
diff	105%	105%	107%	104%	105%	106%	108%	107%	107%	107%	106%

A.0.4 WIFac comparison

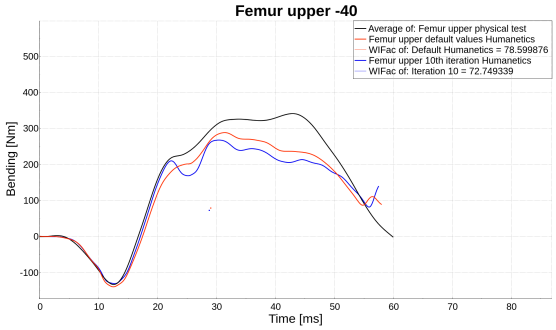

(a) Humanetics

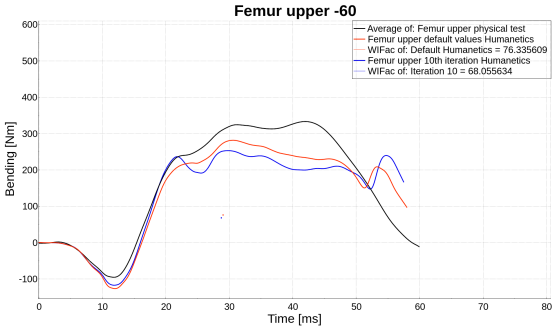

(b) ATD-models

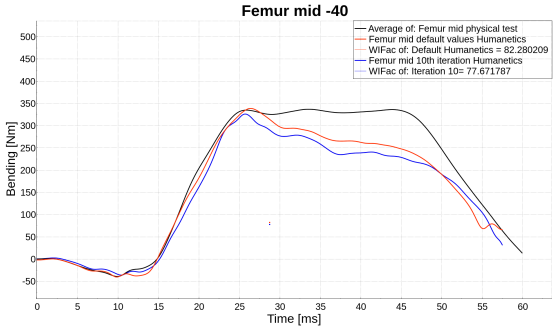

(c) Humanetics

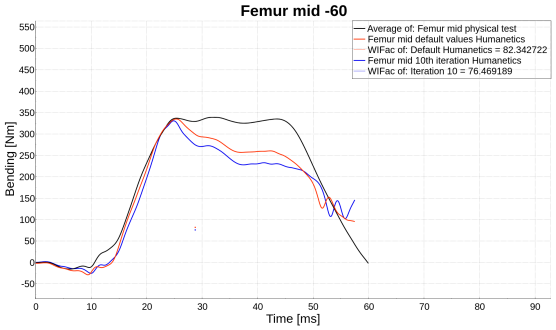

(d) ATD-models

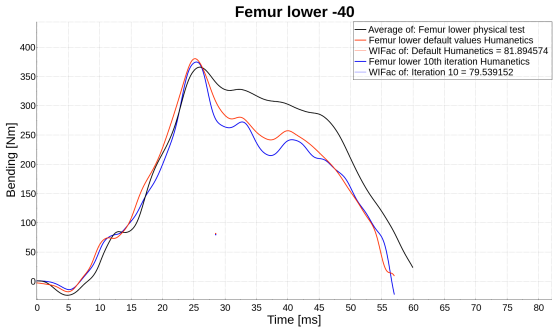

(e) Humanetics

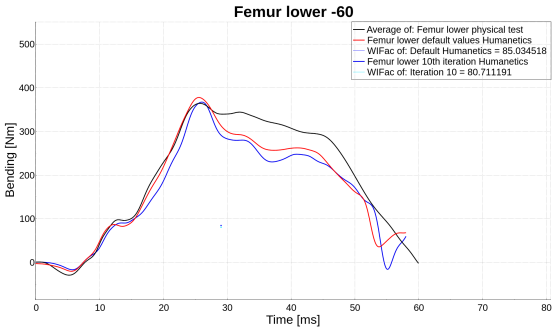

(f) ATD-models

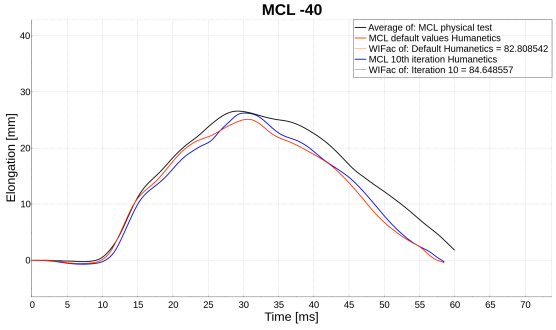

(g) Humanetics

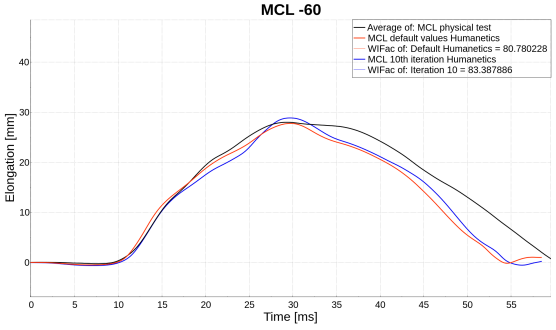

(h) ATD-models

Figure A.3: WIFac comparison between default values and tuned for Humanetics FE aPLI and average physical test values.

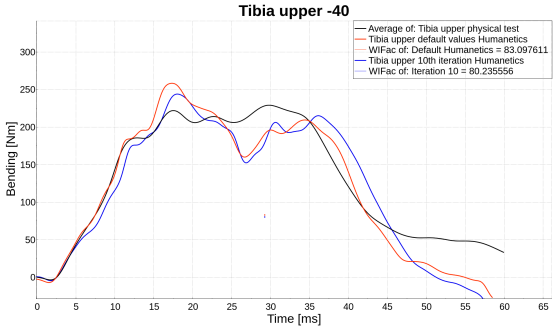

(i) Humanetics

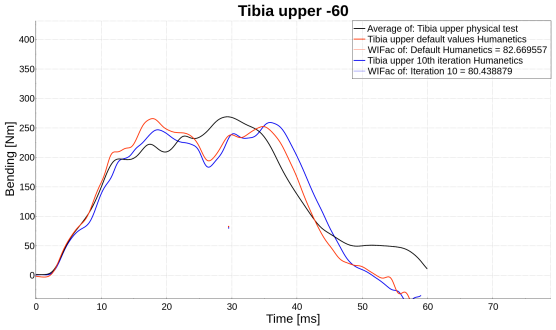

(j) ATD-models

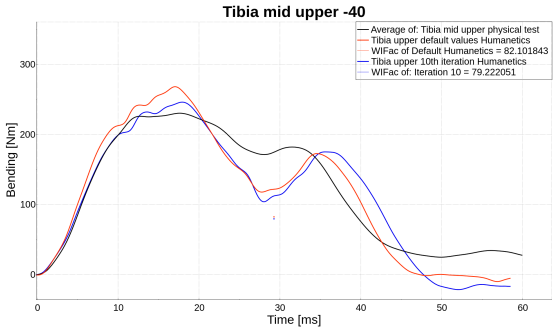

(k) Humanetics

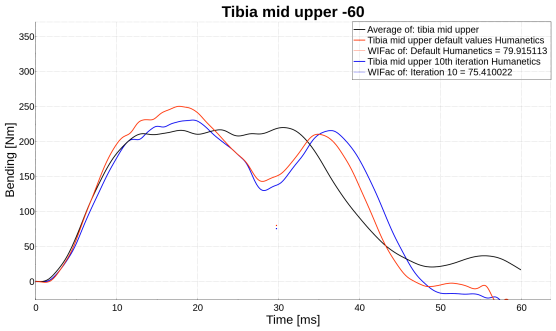

(l) ATD-models

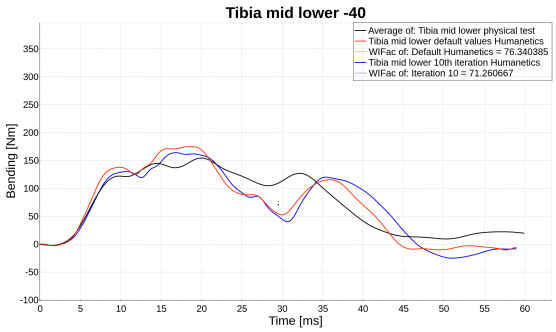

(m) Humanetics

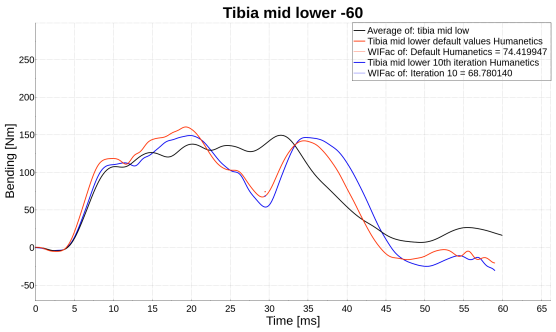

(n) ATD-models

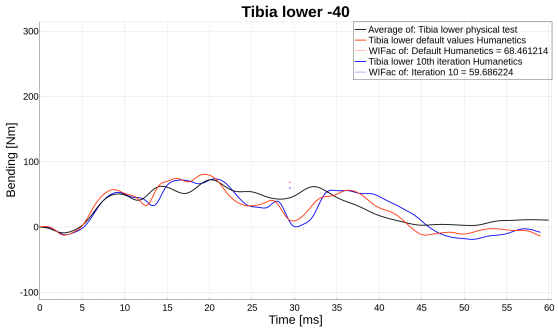

(o) Humanetics

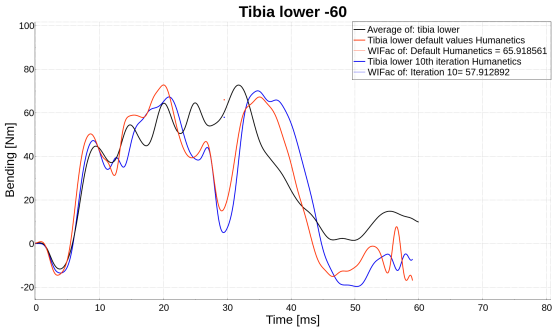

(p) ATD-models

Figure A.3: WIFac comparison between default values and tuned for Humanetics FE aPLI and average physical test values.

DEPARTMENT OF MECHANICS AND MARITIME SCIENCES
CHALMERS UNIVERSITY OF TECHNOLOGY
Gothenburg, Sweden
www.chalmers.se

CHALMERS
UNIVERSITY OF TECHNOLOGY